Modulation of Charge Distribution in Cobalt-α-Diimine Complexes towards Valence Tautomerism

Moya A. Hay[a$], Jett T. Janetzki[a$], Varshini J. Kumar[b], Robert W. Gable[a], Rodolphe Clérac[c], Alyona A. Starikova[d], Paul J. Low[b], and Colette Boskovic [a*]

[a] *School of Chemistry, University of Melbourne, Parkville, Victoria 3010, Australia*

[b] *School of Molecular Sciences, University of Western Australia, 35 Stirling Highway, Crawley, Western Australia 6009, Australia*

[c] *Centre de Recherche Paul Pascal, University of Bordeaux, CNRS, UMR 5031, 33600 Pessac, France.*

[d] *Institute of Physical and Organic Chemistry, Southern Federal University, 344090 Rostov-on-Don, Russian Federation*

*Email: c.boskovic@unimelb.edu.au

$ M.A.H and J.T.J contributed equally to this paper

ABSTRACT

Valence tautomerism (VT) and spin crossover (SCO) are promising avenues through which to develop a range of molecular materials for sensing, memory, and optoelectronic applications. However, these phenomena arise only when specific metal-ligand combinations are employed. The under-explored combination of cobalt(II/III) paired with bis((aryl)imino)acenapthene (Ar-BIAN) ligands, which can exist as neutral Ar-BIAN^{0} (L^{0}), monoanionic radical Ar-BIAN$^{\bullet-}$ ($L^{\bullet-}$), and dianionic Ar-BIAN^{2-} (L^{2-}) forms, has potential to exhibit both VT and SCO. Aiming to develop a new family of switchable molecules, we systematically explored a dual tuning approach by varying the redox-state and aryl substituents in a series of homoleptic $[Co(Ar\text{-}BIAN)_3]^{n+}$ complexes (Ar = Ph, n = 2 (**1**$^{2+}$), 1 (**1**$^{+}$), 0 (**1**); Ar = 3,5-CF_3-Ph, n = 0 (**2**); Ar = 4-MeO-Ph, n = 2 (**3**$^{2+}$), 0 (**3**)). As a prelude to synthetic and experimental studies, density functional theory (DFT) calculations were used to explore the structure and relative energies of the different electronic forms of each complex, comprising different cobalt oxidation and spin states and different ligand oxidation states. Except for compound **3**, DFT identified a HS-Co^{II}-L^{0} containing ground state for all complexes, precluding thermally-induced SCO or VT. For **3**, calculations suggested a possible thermally-accessible LS-Co^{III}-$(L^{\bullet-})_3$ ⇌ HS-Co^{II}-$(L^{\bullet-})_2(L^{0})$ VT interconversion. Experimentally, structural and magnetic data reveal a HS-Co^{II}-L^{0} containing ground state for all six compounds in the solid state, including **3**, discounting thermally-induced VT or SCO. In solution, electrochemical and spectroscopic analysis also indicated that all compounds exist as the HS-Co^{II}-L^{0} containing electromer at 298 K. Intervalence charge transfer (IVCT) bands observed for neutral **1**, **2** and **3** at room temperature indicate the mixed-valent HS-Co^{II}-$(L^{\bullet-})_2(L^{0})$ charge distribution. However, cooling **3** to 243 K in acetonitrile uniquely affords a substantial reduction in the intensity of this IVCT band, consistent with thermally-induced VT interconversion to the LS-Co^{III}-$(L^{\bullet-})_3$

ground state as predicted by DFT calculations. This study emphasizes the utility of computationally guided molecular design for complicated systems with redox activity at the metal and multiple ligands, thus opening new avenues for tuning electronic structure and developing new families of switchable molecules.

INTRODUCTION

Research into molecular materials has flourished over the past several decades, with the potential to facilitate the miniaturization of current technologies.[1–4] To this end, a variety of functional molecules have been investigated within innovative device structures, with a view to introducing, for example, spintronic effects, quantum information processing and sensing behaviour.[5–12] A simple molecular functionality arises from the ability to reversibly switch between energetically accessible states upon application of some stimulus, with accompanying changes in chemical and physical properties.[13–16] The phenomenon of spin crossover (SCO), where coordination compounds undergo a metal-centered spin-state change from low-spin to high-spin in response to change in temperature, pressure or on application of light, has been extensively described in the literature and represents a classic example of such inherently molecular switching behavior.[14,17,18] Further degrees of control over molecular electronic and magnetic properties can be engineered in metal complexes that incorporate redox-active ligands. In certain circumstances, such complexes can be stimulated to switch between meta-stable states through intramolecular metal-ligand charge transfer in a process known as valence tautomerism (VT).[16,19] As a consequence of the complex interplay between metal ion and ligand redox states, valence tautomeric complexes offer fascinating potential for redox (electrical) control of material properties when integrated into devices.[9,20–23]

Cobalt complexes have proven capable of exhibiting either SCO or VT in the presence of a suitable ligand environment.[19,24–26] Spin crossover in cobalt complexes is most prevalent with N-donor ligands,[26,27] the archetypal example being $[Co(terpy)_2]^{2+}$ (terpy = 2,2′:6′,2″-terpyridine),[28–30] and derivatives.[31,32] Whilst valence tautomerism in cobalt systems has been most commonly observed with complexes bearing redox-active O-donor ortho-dioxolene ligands,[16,19] recent reports

of VT in cobalt complexes featuring redox-active N-donor ligands hint at enticing opportunities to expand switchable behavior through the rational design of complexes able to exhibit both SCO and VT.[33,34]

In the context of switching systems with a dual-mode of action, the bis((aryl)imino)acenapthene (Ar-BIAN) ligand family provide a promising basis for exploration.[35–39] The Ar-BIAN ligands are characterized by rich-redox chemistry, comparable to ortho-dioxolene ligands, and are readily accessible in the neutral Ar-BIAN^0 (L^0), monoanionic radical Ar-BIAN$^{\bullet-}$ ($L^{\bullet-}$), and dianionic Ar-BIAN^{2-} (L^{2-}) forms (Scheme 1).[40] Secondly, the straightforward synthesis of these bis(α-diimine) compounds via condensation of acenaphthenequinone with two equivalents of an aryl amine (Ar-NH_2) allows for convenient tuning of the electronic properties via variation of the aryl (Ar) subsitutents,[41] a factor that is important in tuning the relative energies of the different charge distributions.[42–44] An Fe(II) compound has been reported to undergo SCO when coordinated with (bis[(phenyl)imino]acenaphthene) (Ph-BIAN) in the $L^{\bullet-}$ state,[45] and VT has been reported involving the L^{2-} and $L^{\bullet-}$ states of bis[(1,4-bis(2,6-diisopropyl)phenyl)imino]acenaphthene with ytterbium(II/III) and bis[(3,5-bis(dimethyl)phenyl)imino]acenaphthene with vanadium(IV/V).[36,37,46] A density functional theory (DFT) study has also predicted VT behavior in a series of octahedral heteroleptic [Co(Ph-BIAN)(L^{NO})$_2$] and [Co(H-BIAN)(L^{NO})$_2$] complexes (H-BIAN = bis(imino)acenaphthene; L^{NO} = iminovinylketonate ligand) involving the LS-Co^{III}-$L^{\bullet-}$ and HS-Co^{II}-L^0 tautomers.[47] The synthetic challenges associated with preparing the complexes used in those computational studies prompted attention here to be focused on the preparation of a series of homoleptic [Co(Ar-BIAN)$_3$]$^{n+}$ complexes to gain a deeper understanding of the redox

chemistry and how the charge distribution may be influenced by formal redox state and electronic nature of the aryl group.[48]

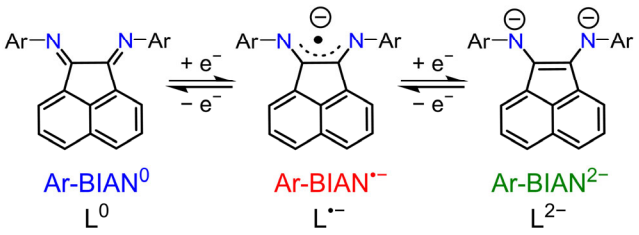

Scheme 1. The neutral Ar-BIAN^0 (L^0), monoanionic Ar-BIAN$^{\bullet-}$ ($L^{\bullet-}$), and dianionic Ar-BIAN^{2-}, (L^{2-}) redox states.

Pursuing a strategy to achieve VT or SCO behaviour in homoleptic Ar-BIAN Co complexes, we adopted a dual approach examining: 1) the impact of the Ar-BIAN oxidation state on the electronic structure of $[Co(Ar\text{-}BIAN)_3]^{n+}$ ($n = 0 – 2$); and 2) the influence of substituents on the Ar-BIAN aryl (Ar) group. Firstly, we focused on the case of complexes derived from Ph-BIAN with the redox ladder $[Co(Ph\text{-}BIAN)_3]^{2+}$ (**1**$^{2+}$), $[Co(Ph\text{-}BIAN)_3]^{+}$ (**1**$^{+}$), and $[Co(Ph\text{-}BIAN)_3]$ (**1**) (Scheme 2). Subsequently, we turned our attention to complexes with the ligands bis[(3,5-bis(trifluoromethyl)phenyl)imino]acenaphthene (3,5-CF_3-Ph-BIAN) and bis[(4-methoxy-phenyl)imino]acenaphthene (4-MeO-Ph-BIAN) which feature electron-withdrawing (CF_3) and electron-donating (OMe) substituents on the aryl rings respectively to isolate compounds: [Co(3,5-CF_3-Ph-BIAN)$_3$)] (**2**), $[Co(4\text{-}MeO\text{-}Ph\text{-}BIAN)_3]$ (**3**), and $[Co(4\text{-}MeO\text{-}Ph\text{-}BIAN)_3]^{2+}$ (**3**$^{2+}$) (Scheme 2). An initial density functional theory (DFT) survey was carried out to identify the most promising VT or SCO candidates. Experimentally, we synthesized the calculated complexes, with the cationic complexes as hexaflurophosphate salts, and conducted a systematic study in both the solid

and solution state. The focus was on establishing the electronic structure (Co oxidation and spin state and ligand oxidation state) adopted by each compound and whether SCO or VT switchable behaviour is evident. The electronic state for the compounds can differ in the solid vs solution state. Through this study of the electronic structure and redox properties of this series of compounds, we achieved the targeted VT behavior and illuminate a strategy to achieve switchable behavior in Co(Ar-BIAN) compounds.

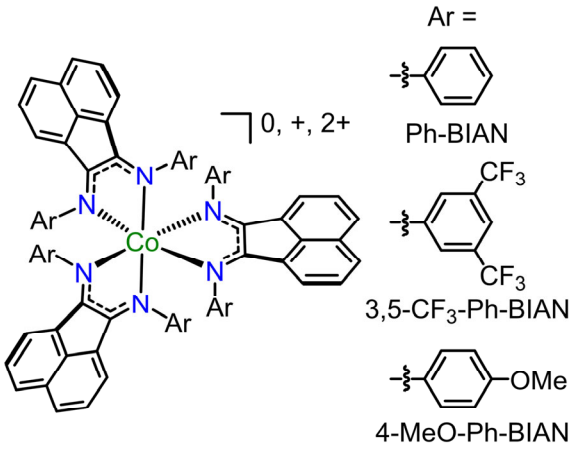

$[Co(Ph\text{-}BIAN)_3]^{2+}$ (**1^{2+}**)

$[Co(Ph\text{-}BIAN)_3]^{+}$ (**1^{+}**)

$[Co(Ph\text{-}BIAN)_3]$ (**1**)

$[Co(3,5\text{-}CF_3\text{-}Ph\text{-}BIAN)_3]$ (**2**)

$[Co(4\text{-}MeO\text{-}Ph\text{-}BIAN)_3]$ (**3**)

$[Co(4\text{-}MeO\text{-}Ph\text{-}BIAN)_3]^{2+}$ (**3^{2+}**)

Scheme 2. Representation of the $[Co(Ar\text{-}BIAN)_3]^{n+}$ (n = 0, 1, 2) complexes and the Ar-BIAN ligands used in this work, with numbering scheme. The cationic complexes were isolated as PF_6^- salts.

RESULTS AND DISCUSSION

Density Functional Theory

To provide a guide prior to synthetic work and experimental studies, an initial survey of the electronic structures their relative stability of $\mathbf{1^{2+}(PF_6)_2}$, $\mathbf{1^{+}(PF_6)}$, **1**, **2**, **3** and $\mathbf{3^{2+}(PF_6)_2}$ was carried out using density functional theory (DFT) calculations based on optimized gas-phase geometries (Tables S1–S3; Figures S1–S6). The electromer energies (E / kcal mol^{-1}) were calculated using the UTPSSh/6-311++G(d,p)[49,50] DFT method (Table S4) with inclusion of zero-point energy (ZPE) in Gaussian 16,[51] a method that has been previously successful in the calculation of electromer energies for cobalt complexes with redox-active ligands.[24,52–55] It is important to note that factors such as lattice effects and solvent can complicate the straight-forward translation of relative energies from calculations performed on isolated molecules in the gas-phase to experimental systems.

For these homoleptic [Co(Ar-BIAN)$_3$]$^{n+}$ complexes, three electronic states were considered in each case. Compounds $\mathbf{1^{2+}(PF_6)_2}$ and $\mathbf{3^{2+}(PF_6)_2}$ can adopt HS-Co^{II}-(L^0)$_3$, LS-Co^{II}-(L^0)$_3$ or LS-Co^{III}-(L$^{\bullet-}$)(L^0)$_2$; $\mathbf{1^{+}(PF_6)}$ can adopt HS-Co^{II}-(L$^{\bullet-}$)(L^0)$_2$, LS-Co^{II}-(L$^{\bullet-}$)(L^0)$_2$ or LS-Co^{III}-(L$^{\bullet-}$)$_2$(L^0); and **1**, **2**, **3** can adopt HS-Co^{II}-(L$^{\bullet-}$)$_2$(L^0), LS-Co^{II}-(L$^{\bullet-}$)$_2$(L^0) or LS-Co^{III}-(L$^{\bullet-}$)$_3$. For simplification we refer to the states in abbreviated form as containing HS-Co^{II}-L^0, LS-Co^{II}-L^0, or LS-Co^{III}-L$^{\bullet-}$ moieties.

In general, thermally-induced SCO and VT intercoversions would require respective LS-Co^{II}-L^0 and LS-Co^{III}-L$^{\bullet-}$ ground states and the HS-Co^{II}-L^0 containing tautomer destabilized by no more than 12 kcal mol^{-1}.[52,54] Thermally induced SCO and VT are both entropically driven, with

the HS-Co^{II}-L^0 containing electromer favored upon increasing temperature due to the increase in entropy associated with the longer bond lengths, higher vibrational density of states, and greater spin-degeneracy of the charge distribution.[19]

The Ph-BIAN redox family of compounds (**$1^{2+}(PF_6)_2$**, **$1^{+}(PF_6)$**, and **1**) were first investigated to examine the impact of successive reductions of the Ph-BIAN ligands on the relative energies of the different electromers (Figure 1). In all three cases, the HS-Co^{II}-L^0 containing electromer was found to be the ground state, with the LS-Co^{II}-L^0 and LS-Co^{III}-$L^{\bullet-}$ containing electromers at higher energies. Thus, the calculations suggest that **$1^{2+}(PF_6)_2$**, **$1^{+}(PF_6)$**, and **1** should remain in the HS-Co^{II}-L^0 containing state at all temperatures with no possibility of either VT or SCO interconversions.

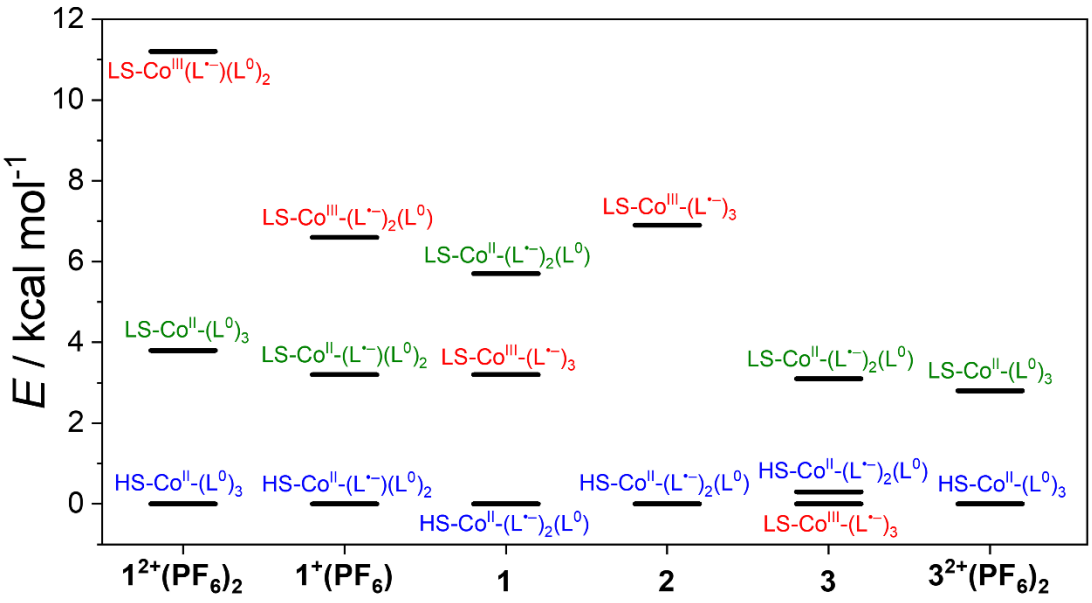

Figure 1. Calculated relative energies of the three different electronic forms for the cobalt Ar-BIAN complexes in compounds **$1^{2+}(PF_6)_2$**, **$1^{+}(PF_6)$** **1**, **2**, **3**, and **$3^{2+}(PF_6)_2$** calculated by DFT (UTPSSh/6-311++G(d,p)) with zero-point energy.

However, the relative energy of the LS-Co^{III}-$L^{\bullet-}$ containing electromer decreases with the total charge of the complex, following $\mathbf{1^{2+}(PF_6)_2} > \mathbf{1^{+}(PF_6)} > \mathbf{1}$ (Figure 1). This is attributed to the increasing electron donation arising from successive introduction of anionic Ph-BIAN$^{\bullet-}$ ligands that stabilizes the shorter bond lengths associated with LS-Co^{III}. This provides a critical insight for accessing VT as it suggest that neutral [Co(Ar-BIAN)$_3$] complexes are more promising than the cationic complexes for achieving the LS-Co^{III}-$L^{\bullet-}$ containing ground state necessary for a LS-Co^{III}-$L^{\bullet-}$ ⇌ HS-Co^{II}-L^0 based VT interconversion. On the other hand, a LS-Co^{II}-L^0 ground state and subsequent SCO appears to be inaccessible with this family. These observations prompted explorations of variation of substituents on the Ar-BIAN ligand to further stabilize the LS-Co^{III}-$L^{\bullet-}$ state, focusing on the neutral compounds. Neutral compounds [Co(3,5-CF_3-Ph-BIAN)$_3$] (**2**) and [Co(4-MeO-Ph-BIAN)$_3$] (**3**), containing Ar-BIAN ligands with the most electron-withdrawing and donating substituents respectively, were selected for further exploration.[56,57]

The DFT calculations of complex **2** indicate that the electron-withdrawing 3,5-CF_3-Ph-BIAN ligand significantly destabilizes the LS-Co^{III}-$(L^{\bullet-})_3$ electromer from the HS-Co^{II}-$(L^{\bullet-})_2(L^0)$ ground state (Figure 1) and thus VT is not accessible. In contrast, the strongly electron-donating methoxy groups of 4-MeO-Ph-BIAN in complex **3** results in reversal of the energy ordering of the states and afford the LS-Co^{III}-$(L^{\bullet-})_3$ tautomer as lowest in energy, albeit with the HS-Co^{II}-$(L^{\bullet-})_2(L^0)$ state in very close proximity (0.3 kcal mol^{-1}). This suggests the possibility of a thermally induced LS-Co^{III}-$(L^{\bullet-})_3$ ⇌ HS-Co^{II}-$(L^{\bullet-})_2(L^0)$ VT interconversion (Scheme 3) for **3**.

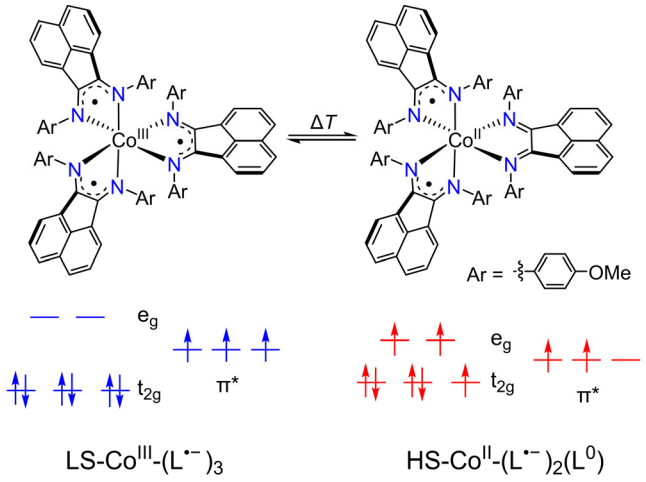

Scheme 3. Valence tautomeric equilibria predicted for **3** via DFT.

Neutral [Co(Ar-BIAN)$_3$] complexes with several other aryl substituents with a range of Hammett σ-parameters were also explored (Figure S7), with a clear linear trend showing stabilization of the LS-Co^{III}-(L$^{\bullet-}$)$_3$ state with increasing electron-donation (Figure S8). The ground state of **3**$^{2+}$**(PF$_6$)$_2$**, as in the case of **1**$^{2+}$**(PF$_6$)$_2$**, was found to be the HS-Co^{II}-(L^0)$_3$ electromer, with the LS-Co^{II}-(L^0)$_3$ electromer relatively destabilized (Figure 1). In addition, for **3**$^{2+}$**(PF$_6$)$_2$**, numerous attempts to find the LS-Co^{III}-(L$^{\bullet-}$)(L^0)$_2$ electromer invariably gave the LS-Co^{II}-(L^0)$_3$ state at potential energy surface of the same multiplicity (S = 1/2) due to the symmetric structure being more energy preferable. The computational results thus clearly suggest that of the compounds investigated here, the combination of the maximum number of Ar-BIAN$^{\bullet-}$ ligands and electron-donating ligand substituents accessed in **3** afford the best prospects for achieving valence tautomerism.

Exchange coupling parameters can alter the relative energy stabilization of the different charge distributions and must be considered for electromers where at least two open shell sites (HS-Co^{II}, LS-Co^{II}, and $L^{\bullet-}$) are present (excludes all electromers of dicationic compounds $\mathbf{1^{2+}(PF_6)_2}$ and $\mathbf{3^{2+}(PF_6)_2}$). Exchange spin coupling parameters J ($-2JS_1 \cdot S_2$ formalism) were estimated using the Broken Symmetry (BS) approximation (Table S5).[58] In this method, the calculated exchange is isotropic, and does not consider spin-orbit coupling (SOC) contributions. Unfortunately, at the level of theory employed, an exact value of the exchange cannot be conclusively inferred, particularly in the case of anisotropic ions such as HS-Co^{II}.[43,59,60] However, it is nonetheless important to consider due to the likelihood of magnetic exchange interactions in such systems.

For compound $\mathbf{1^{+}(PF_6)}$, in the HS-Co^{II}-$(L^{\bullet-})(L^0)_2$ state, very strong antiferromagnetic exchange (–620 cm^{-1}) was calculated between HS-Co^{II} and $L^{\bullet-}$, whereas weaker ferromagnetic exchange (39 cm^{-1}) was predicted between LS-Co^{II} and $L^{\bullet-}$ in the LS-Co^{II}-$(L^{\bullet-})(L^0)_2$ state. For the LS-Co^{III}-$(L^{\bullet-})_2(L^0)$ electromer of $\mathbf{1^{+}(PF_6)}$, only a moderate antiferromagnetic $L^{\bullet-}\cdots L^{\bullet-}$ interaction (–21 cm^{-1}) was calculated. For compound **1**, the HS-Co^{II}-$(L^{\bullet-})_2(L^0)$ tautomer is suggested to have strong antiferromagnetic exchange (–143 cm^{-1}) between the HS-Co^{II} center and the $L^{\bullet-}$ ligands, as well as a competing strong antiferromagnetic $L^{\bullet-}\cdots L^{\bullet-}$ interaction (–218 cm^{-1}). For the LS-Co^{II}-$(L^{\bullet-})_2(L^0)$ state of **1**, a strong ferromagnetic exchange (400 cm^{-1}) is instead predicted between the LS-Co^{II} center and the $L^{\bullet-}$ ligands, with a moderate $L^{\bullet-}\cdots L^{\bullet-}$ ferromagnetic exchange (47 cm^{-1}). In the LS-Co^{III}-$(L^{\bullet-})_3$ electromer of **1**, moderate ferromagnetic exchange is calculated (32 cm^{-1}) between the $L^{\bullet-}$ ligands. The magnitude and sign of the exchange coupling parameters for the three analogous electromers in compounds **2** and **3** are similar to those of **1** (Table S5). For the

HS-Co^{II}-$(L^{\bullet-})_2(L^0)$ electromers of **2** and **3**, again antiferromagnetic HS-$Co^{II}\cdots L^{\bullet-}$ (–76 and –498 cm^{-1} respectively) and $L^{\bullet-}\cdots L^{\bullet-}$ (–401 and –30 cm^{-1} respectively) interactions were estimated. However, contrary to **1** and **2**, calculations for **3** suggested a significantly more dominant HS-$Co^{II}\cdots L^{\bullet-}$ exchange interaction. As per **1**, the $L^{\bullet-}\cdots L^{\bullet-}$ exchange in the LS-Co^{III}-$(L^{\bullet-})_3$ electromer for **2** (50 cm^{-1}) and **3** (46 cm^{-1}) is calculated to be weakly ferromagnetic. For the LS-Co^{II}-$(L^{\bullet-})_2(L^0)$ state of **3**, similar strong ferromagnetic LS-$Co^{II}\cdots L^{\bullet-}$ and $L^{\bullet-}\cdots L^{\bullet-}$ interactions (493 and 112 cm^{-1} respectively) is obtained from the calculations. For **1**, **2** and **3**, the strong exchange interactions (Table S5) predicted for the different energetically accessible electromers are expected to have a pronounced impact on the experimentally observed charge distributions. For example, if compounds **1**, **2**, and/or **3** are isolated in the HS-Co^{II}-$(L^{\bullet-})_2(L^0)$ charge distribution, the predicted large antiferromagnetic HS-$Co^{II}\cdots L^{\bullet-}$ and $L^{\bullet-}\cdots L^{\bullet-}$ exchange interactions may result in lower-than-expected magnetic response.

The combined DFT results therefore set out a series of structure property relationships and predictions of the electronic and magnetic properties of this family of Ar-BIAN complexes in their various redox states. Of the six compounds calculated, the most promising candidate for achieving molecular switchability was determined to be neutral compound **3**, which is calculated to have the necessary energy ordering of the LS-Co^{III}-$(L^{\bullet-})_3$ and HS-Co^{II}-$(L^{\bullet-})_2(L^0)$ electromers to possibly achieve thermally-induced VT (Scheme 3). Next, our attention turned to experimental verification, with a focus on establishing the electronic state of the six compounds in the solid and solution state, as well as determining whether **3** displays thermally-induced VT.

Synthesis

As detailed in the Supporting Information, compounds $\mathbf{1^{2+}(PF_6)_2}$ and $\mathbf{3^{2+}(PF_6)_2}$ were synthesized by reacting cobalt acetate ($Co(OAc)_2$) with three equivalents of Ph-BIAN or 4-MeO-Ph-BIAN in air, with subsequent addition of two equivalents of PF_6^- as the counterion, yielding a red precipitate. The compound was recrystallized by layering a concentrated dichloroethane (DCE) solution with diisopropyl ether (*i*Pr$_2$O). The higher boiling point DCE and *i*Pr$_2$O solvents (compared to dichloromethane and diethyl ether) were chosen to limit solvent loss from the bulk crystalline sample. Compound $\mathbf{1^+(PF_6)}$ was synthesized in tetrahydrofuran (THF) under N_2 by firstly forming complex $[Co(Ph\text{-}BIAN)]^{2+}$, followed by reduction with one equivalent of cobaltocene ($CoCp_2$). The product was isolated as the PF_6^- salt and recrystallized from acetonitrile (MeCN) and diethyl ether (Et_2O). An analytically pure bulk sample of $\mathbf{1^+(PF_6)}$ could not be consistently obtained due to its similar solubility with the $(CoCp_2)(PF_6)$ byproduct.

Synthesis of neutral **2** was achieved by reaction of six equivalents of 3,5-CF_3-Ph-BIAN with $Co_2(CO)_8$, in toluene under N_2, in a process that leads to in situ reduction of 3,5-CF_3-Ph-BIAN by the Co(0) source. The complex was subsequently isolated as dark purple crystals. Compound **2** has been previously reported from a different synthetic method,[61] and whilst originally formulated as $[Co^I(3,5\text{-}CF_3\text{-}Ph\text{-}BIAN^{\bullet-})(3,5\text{-}CF_3\text{-}Ph\text{-}BIAN^0)_2]$, consideration of the crystallographically determined bond lengths suggests that this description is not definitive (see Structure Description section). Attempts to synthesize neutral **1** and **3** using the same procedure for **2** yielded a mixture of products, presumably due to the lower reduction potentials of Ph-BIAN and 4-MeO-Ph-BIAN. Instead, a comproportionation approach was developed. Reaction of a 2:1 combination of Ar-BIAN and Ar-$BIAN^{2-}$ (Ar = Ph and 4-MeO-Ph) resulted in formation of two equivalents of Ar-$BIAN^{\bullet-}$ and one Ar-BIAN. Subsequent addition of $Co(OAc)_2$ to this ligand

mixture allowed formation and isolation of neutral compounds **1** and **3**. The compounds were separated from NaOAc by-product by extraction of the compound into toluene, and then washing with ethanol. Elemental and thermogravimetric analysis (Figure S9) confirmed purity and solvation of all five compounds (**1**, **2**, **3**, $\mathbf{1}^{2+}\mathbf{(PF_6)_2}$, $\mathbf{3}^{2+}\mathbf{(PF_6)_2}$). In solution, **1**, **2** and **3** are highly air-sensitive and decompose after 4-5 hours even under inert conditions.

Structure Description

Structures of $\mathbf{1}^{2+}\mathbf{(PF_6)_2}$, $\mathbf{1}^{+}\mathbf{(PF_6)}$, **1**, **2**, **3** and $\mathbf{3}^{2+}\mathbf{(PF_6)_2}$ were determined by single crystal X-ray diffraction (Table S6, S7) to aid in determining the electronic state adopted by each complex in the solid-state. Data were collected at 100 K for compounds $\mathbf{1}^{2+}\mathbf{(PF_6)_2}$, $\mathbf{1}^{+}\mathbf{(PF_6)}$, **1**, **2**, and $\mathbf{3}^{2+}\mathbf{(PF_6)_2}$, and at 120 K for **3**. As the collection temperature will influence the electromeric state of a compound if it displays thermal VT or SCO, each structure was collected in the same low temperature range (100–120 K) to access the ground state. Multiple attempts were made to collect data for the poorly diffracting crystals of **1** and **3** using synchrotron radiation (detailed in the Supporting Information),[62,63] and as such the *R*-values are higher.

The presence of solvent in the crystal structures is consistent with the compositions $\mathbf{1}^{2+}\mathbf{(PF_6)_2}$·2.5DCE·1.5*i*Pr$_2$O, $\mathbf{1}^{+}\mathbf{(PF_6)}$·2Et$_2$O·0.6MeCN, **1**·2.5THF·pentane, **2**·tol, **3** and $\mathbf{3}^{2+}\mathbf{(PF_6)_2}$·DCE as detailed in the Supporting Information. Compound $\mathbf{1}^{2+}\mathbf{(PF_6)_2}$·2.5DCE·1.5*i*Pr$_2$O crystallizes with two independent Co complexes in the structure, which are labelled $\mathbf{1}^{2+}$**A** and $\mathbf{1}^{2+}$**B** in the discussion below. The formulae in the crystal structure differ from those the bulk samples, which analyzed as $\mathbf{1}^{2+}\mathbf{(PF_6)_2}$·0.5DCE·0.5*i*Pr$_2$O, **1**·0.8EtOH, **2**, **3**·EtOH, $\mathbf{3}^{2+}\mathbf{(PF_6)_2}$·DCE. For complexes $\mathbf{1}^{2+}\mathbf{(PF_6)_2}$, **2**, and $\mathbf{3}^{2+}\mathbf{(PF_6)}_2$, this arises from partial desolvation upon collection of the

bulk sample, and for **1** and **3**, the different methods by which the single-crystal and bulk samples were obtained. Powder X-ray diffraction (PXRD) confirmed the phase purity of the bulk samples and matched with the diffraction pattern calculated from the single-crystal X-ray structural analysis (Figures S10-S12). Despite the inability to reliably obtain a pure bulk of $\mathbf{1^{+}(PF_6)}$, we have included the single-crystal data for the purposes of assisting with bond length analysis.

In the solid-state structures, all the metal complexes possess approximate D_3 point symmetry and share a Co(Ar-BIAN)$_3$ motif, with the cobalt center coordinated by three bidentate Ar-BIAN ligands, giving a distorted octahedral coordination geometry (Figure 2, S13–S15). For the neutral compounds (**1**, **2**, and **3**), the asymmetric unit comprises half a molecule of [Co(Ar-BIAN)$_3$], in contrast to compounds $\mathbf{1^{2+}(PF_6)_2}$, $\mathbf{1^{+}(PF_6)}$ and $\mathbf{3^{2+}(PF_6)_2}$, which contain a full molecule with three crystallographically inequivalent Ar-BIAN ligands. The oxidation and spin state of the cobalt center can be determined by the Co−N bond lengths, bond valence sum (BVS) parameters (Table S8),[64] octahedral distortion parameters (Σ, Θ)[65] and the octahedral *SHAPE* index (Table 1).[66] In general, Co−N bond lengths and octahedral distortions increase following the trend LS-Co^{III} < LS-Co^{II} < HS-Co^{II}. The oxidation state of the Ar-BIAN ligands can be assigned via analysis of the α-diimine C–N and C–C bonds.[40,45,61,67–69] The monoanionic $L^{\bullet-}$ state has longer C–N and shorter C–C bonds compared to the neutral L^0 form as a result of populating formally π* orbitals.

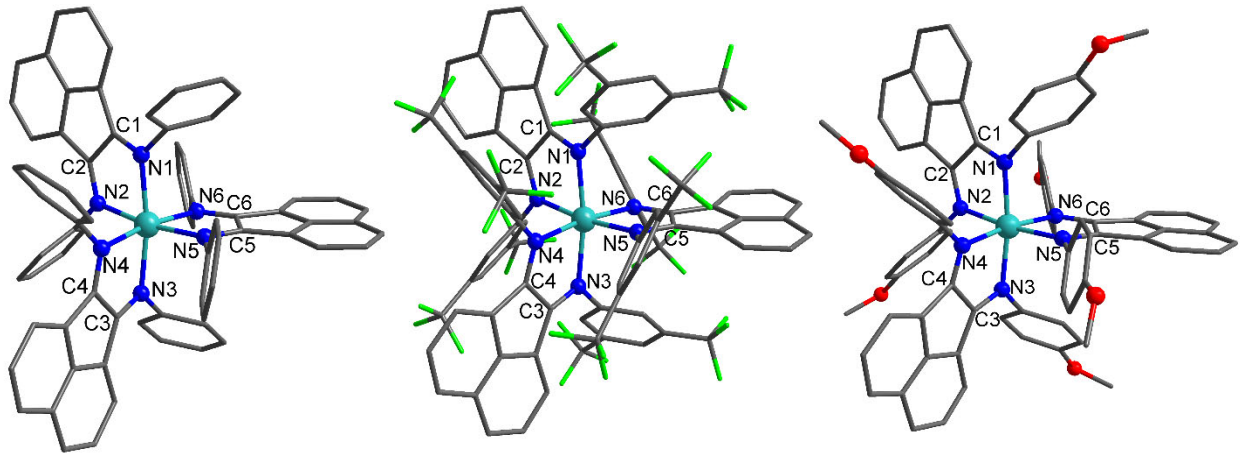

Figure 2. Molecular structures of neutral complexes **1** (100 K) (left), **2** (100 K) (middle), and **3** (120 K) (right) as determined via single-crystal X-ray diffraction with relevant atoms labelled. Hydrogen atoms and solvent molecules have been omitted for clarity. Color code: C (dark grey), N (blue), O (red), Co (light blue), F (green).

Table 1. Selected interatomic distances (Å), distortion parameters, and BVS values for $\mathbf{1^{2+}(PF_6)_2}$·2.5DCE·1.5iPr$_2$O (molecules A and B), $\mathbf{1^{+}(PF_6)}$·2Et$_2$O·0.6MeCN, **1**·2.5THF·pentane, **2**·tol, **3** and $\mathbf{3^{2+}(PF_6)_2}$·DCE.

	$\mathbf{1^{2+}(PF_6)_2}$ **A**	$\mathbf{1^{2+}(PF_6)_2}$ **B**	$\mathbf{1^{+}(PF_6)}$	**1**	**2**	**3**	$\mathbf{3^{2+}(PF_6)_2}$
Temperature (K)	100	100	100	100	100	120	100
			interatomic distances				
Co–N_1	2.127(2)	2.152(2)	2.112(2)	2.142(4)	2.114(2)	2.182(4)	2.120(3)
Co–N_2	2.154(2)	2.163(2)	2.127(2)	2.116(4)	2.135(2)	2.114(5)	2.141(3)
Co–N_3	2.133(2)	2.156(2)	2.137(2)	2.142(4)	2.114(2)	2.182(4)	2.123(3)
Co–N_4	2.123(2)	2.128(2)	2.152(2)	2.116(4)	2.135(2)	2.114(5)	2.120(3)
Co–N_5	2.159(2)	2.133(2)	2.104(2)	2.096(4)	2.131(2)	2.106(5)	2.142(3)
Co–N_6	2.150(2)	2.124(2)	2.123(2)	2.096(4)	2.131(2)	2.106(5)	2.135(3)
Co–N_{avg}	2.141(2)	2.143(2)	2.126(2)	2.118(4)	2.126(2)	2.134(5)	2.131(3)
C_1–N_1	1.288(3)	1.280(3)	1.296(3)	1.299(6)	1.302(3)	1.300(6)	1.286(5)
C_2–N_2	1.283(3)	1.275(3)	1.297(3)	1.305(5)	1.303(3)	1.318(7)	1.298(5)
C_3–N_3	1.283(3)	1.282(3)	1.290(3)	1.299(6)	1.302(3)	1.300(6)	1.282(5)
C_4–N_4	1.276(3)	1.278(3)	1.286(3)	1.305(5)	1.303(3)	1.318(7)	1.286(5)
C_5–N_5	1.278(4)	1.283(3)	1.297(2)	1.284(5)	1.330(3)	1.279(7)	1.288(5)
C_6–N_6	1.277(4)	1.273(3)	1.303(3)	1.284(5)	1.330(3)	1.279(7)	1.290(5)
C_1–C_2	1.522(3)	1.509(3)	1.483(3)	1.460(7)	1.481(3)	1.449(8)	1.504(5)
C_3–C_4	1.508(4)	1.517(3)	1.493(2)	1.460(7)	1.481(3)	1.449(8)	1.511(5)
C_5–C_6	1.512(4)	1.507(4)	1.479(3)	1.474(9)	1.440(4)	1.50(1)	1.508(5)
Co···Co [a]	12.133(1)		16.897(1)	10.914(2)	11.6148(2)	10.807(2)	10.826(5)
			distortion and oxidation state parameters				
SHAPE (O_h) [b]	1.088	1.116	1.277	1.180	1.119	1.216	0.987
$\boldsymbol{\Sigma}$/° [c]	75.9	76.8	76.9	75.3	74.8	74.9	70.3
$\boldsymbol{\Theta}$/° [c]	233.9	237.5	242.1	239.9	242.0	237.2	229.2
BVS[d]	1.93	1.88	2.00	2.08	2.00	1.97	1.98

[a]Closest intermolecular distance. [b]SHAPE index for octahedral geometry in *SHAPE 2.1*.[66] A **value of 0 represents a perfect octahedron.** [c]Σ = the sum of the deviation of the twelve N−Co−N angles from 90°. Θ = sum of the deviation of 24 unique torsional angles between the N atoms on opposite triangular faces of the octahedron from 60°, providing the degree of trigonal distortion from an octahedron to trigonal prism. These were calculated using OctaDist - a program for determining the structural distortion of the octahedral complexes. For a perfect octahedron, $\boldsymbol{\Sigma}$, and $\boldsymbol{\Theta}$ are zero.[65] [d]Value close to 2 indicates Co^{II} and 3 for Co^{III}.[64,70,71]

Analysis of the average Co−N bond lengths (Co−N_{avg}) and octahedral distortion parameters for $\mathbf{1^{2+}A}$ and $\mathbf{1^{2+}B}$ in $\mathbf{1^{2+}(PF_6)_2}$·2.5DCE·1.5*i*Pr$_2$O, $\mathbf{1^{+}(PF_6)}$·2Et$_2$O·0.6MeCN, **1**·2.5THF·pentane, **2**·tol, **3** and $\mathbf{3^{2+}(PF_6)_2}$·DCE (Table 1) indicates the oxidation and spin state adopted by the cobalt center in each complex in the solid-state. The Co−N_{avg} bond lengths and lack of Jahn-Teller distortions in $\mathbf{1^{2+}(PF_6)_2}$ and $\mathbf{3^{2+}(PF_6)_2}$ at 100 K are consistent with HS-Co^{II}, and are in good agreement with the DFT optimized geometry values for the HS-Co^{II}-$(L^0)_3$ state, as opposed to LS-

Co^{II}-$(L^0)_3$ or LS-Co^{III}-$(L^{\bullet-})(L^0)_2$ (Tables S1 and S3). Likewise in compound $\mathbf{1^+(PF_6)}$, the Co–N_{avg} bond lengths and absence of Jahn-Teller distortions are also consistent with HS-Co^{II}, with bond lengths in good agreement with the DFT calculated lengths for the HS-Co^{II}-$(L^{\bullet-})(L^0)_2$ state (Tables S1). Thus, crystallographic data at 100 K indicate a HS-Co^{II}-$(L^0)_3$ electromeric state for $\mathbf{1^{2+}(PF_6)_2}$ and $\mathbf{3^{2+}(PF_6)_2}$, and a HS-Co^{II}-$(L^{\bullet-})(L^0)_2$ state for $\mathbf{1^+(PF_6)}$.

The experimental Co–N_{avg} bond lengths, BVS and distortion parameters for compound **1** and **3**, collected at 100 and 120 K respectively, are consistent with HS-Co^{II} (Table S2 and S3). The experimental Co–N_{avg} bond lengths for compound **2** at 100 K are intermediate between the DFT optimized geometries for the HS-Co^{II}-$(L^{\bullet-})_2(L^0)$ and LS-Co^{III}-$(L^{\bullet-})_3$ states (Table S2). However, in conjunction with BVS analysis and distortion parameters, a HS-Co^{II} center is still suggested. In previous work, compound **2** was assigned the electronic state [Co^{I}(3,5-CF_3-Ph-BIAN$^{\bullet-}$)(3,5-CF_3-Ph-BIAN$^0)_2$] based on structural analysis.[61] However, attempts to locate the [Co^{I}(3,5-CF_3BIAN$^{\bullet-}$)(3,5-CF_3-Ph-BIAN$^0)_2$] state using DFT were unsuccessful, suggesting that Co^{I} is too high in energy.

The three neutral compounds **1**, **2** and **3** are also assigned as having a HS-Co^{II} center based on bond length, BVS and distortion parameter analysis. However, they all show some suggestion of Jahn-Teller distortion in the experimental values, typical of LS-Co^{II}.[26,27,71] This is most obvious for **3**, while more subtle for **1** and **2**. It is possible that the slightly higher (120 K) collection temperature for **3** compared to **1** and **2** (100 K) is the reason for the more obvious elongation. In all cases, the distortion is not to the extent indicated by the DFT optimized geometry of the LS-Co^{II}-$(L^{\bullet-})_2(L^0)$ state (Table S9). This could be due to 1) a disorder (either static or dynamic) of the Jahn-Teller distortion as previously observed for LS-Co^{II} or 2) a mixture of the LS and HS-Co^{II} at

the measured temperatures.[28,71] In all three cases, the experimental values are closer to the geometry optimized HS-Co^{II}-$(L^{\bullet-})_2(L^0)$ geometry than LS-Co^{II}-$(L^{\bullet-})_2(L^0)$, suggesting a mixture of spin states (Table S9). To estimate the fraction of LS-Co^{II} present, we compared the difference between the Co−N_{axial} and Co−$N_{equatorial}$ (averaged) lengths for the geometry optimized structure versus the experimentally obtained bond-lengths (details in SI). This gave an approximate LS-Co^{II} percentage of 16% for **1**, 8% for **2**, and 33% for **3**. Although only an approximation, especially considering the higher *R*-values for **1** and **3**, the analysis of the experimental data for **1**, **2** and **3** suggests divalent cobalt, with dominant HS-Co^{II}, ruling out the possibility of LS-Co^{III} at the measured temperature. Overall compounds **1**, **2** and **3** can be assigned as the HS-Co^{II}-$(L^{\bullet-})_2(L^0)$ electromer in the solid-state at 100 or 120 K.

Confirmation that the solid-state electronic configuration $\mathbf{1^{2+}(PF_6)_2}$ and $\mathbf{3^{2+}(PF_6)_2}$ is HS-Co^{II}-$(L^0)_3$, $\mathbf{1^{+}(PF_6)}$ is HS-Co^{II}-$(L^{\bullet-})(L^0)_2$, and **1**, **2** and **3** are HS-Co^{II}-$(L^{\bullet-})_2(L^0)$ at 100 or 120 K, based on the cobalt center spin and oxidation state assignment, is provided by the bond length analysis and oxidation-state assignment of the Ar-BIAN ligands. The α-diimine C–N and C–C bond distances for each Ar-BIAN in $\mathbf{1^{2+}A}$ and $\mathbf{1^{2+}B}$, and $\mathbf{3^{2+}(PF_6)_2}$ are consistent with neutral Ar-$BIAN^0$ oxidation state,[45,48] confirming the HS-Co^{II}-$(L^0)_3$ charge distribution at 100 K in the solid-state. The π-acceptor capacity of neutral Ph-BIAN and 4-MeO-Ph-BIAN is illustrated by the observed shortening of the C–C bond and elongation of the C–N bonds experimentally upon coordination compared to uncoordinated Ph-BIAN (C–N bond distance 1.275 Å, C–C bond distance 1.526 Å) and 4-MeO-Ph-BIAN (C–N bond distance 1.277 Å, C–C bond distance 1.527 Å).[45,72]

On comparing the α-diimine bond distances of the redox series of compounds $\mathbf{1^{2+}(PF_6)_2}$, $\mathbf{1^{+}(PF_6)}$, **1** (Figure 3) at 100 K, an elongation of the C−N bonds and a contraction of the C−C bond

is observed with increased equivalents of Ph-BIAN$^{\bullet-}$. In compound **1^{+}(PF$_6$)**, the C–N and C–C bond lengths lie between the values expected for Ph-BIAN^{0} and Ph-BIAN$^{\bullet-}$,[40,45,61,67] and arise from the presence of a single L$^{\bullet-}$ and two L^{0} ligands either crystallographic disordered or electronically delocalized. This confirms the electromer state adopted by **1^{+}(PF$_6$)** as HS-Co^{II}-(L$^{\bullet-}$)(L^{0})$_2$ in the solid-state at 100 K. The C−N and C−C bonds of **1** are further elongated and contracted, respectively, while still lying between the values expected for Ph-BIAN^{0} and Ph-BIAN$^{\bullet-}$, confirming the mixed-valent HS-Co^{II}-(L$^{\bullet-}$)$_2$(L^{0}) state at 100 K in the solid-state. The same observation is made for **2** at 100 K. For compound **3**, shorter experimentally observed C−C and C−N bonds compared to **3^{2+}(PF$_6$)$_2$**, that are still too long and short for pure 4-MeO-Ph-BIAN$^{\bullet-}$ indicate two L$^{\bullet-}$ and one L^{0} ligands, confirming HS-Co^{II}-(L$^{\bullet-}$)$_2$(L^{0}) state at 120 K. Overall, structural analysis thus confirms that in the solid-state at 100 K (**3** at 120 K), the electromeric state of **1^{2+}(PF$_6$)$_2$** and **3^{2+}(PF$_6$)$_2$** are HS-Co^{II}-(L^{0})$_3$, **1^{+}(PF$_6$)** is HS-Co^{II}-(L$^{\bullet-}$)(L^{0})$_2$, and **1**, **2** and **3** is HS-Co^{II}-(L$^{\bullet-}$)$_2$(L^{0}). Compound **3**, predicted to have a LS-Co^{III}-(L$^{\bullet-}$)$_3$ ground state by DFT, adopts a HS-Co^{II}-(L$^{\bullet-}$)$_2$(L^{0}) ground-state in the solid sample.

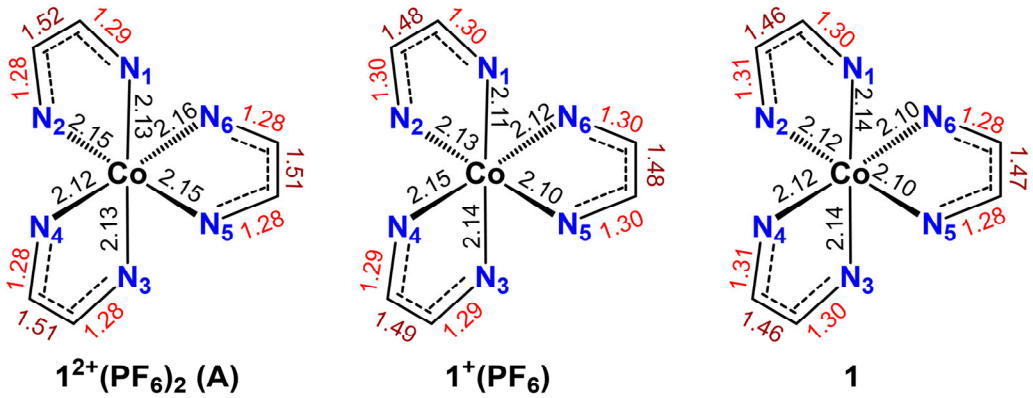

1^{2+}(PF$_6$)$_2$ (A) **1^{+}(PF$_6$)** **1**

Figure 3. Comparison of bond lengths observed for **1^{2+}(PF$_6$)$_2$ (A), 1^{+}(PF$_6$)** and **1** at 100 K used to assign oxidation states.

Infrared Spectroscopy

Infrared (IR) spectra of $\mathbf{1}^{2+}(\mathbf{PF_6})_2$·0.5DCE·0.5*i*Pr$_2$O, **1**·0.8EtOH, **2**, **3**·EtOH, $\mathbf{3}^{2+}(\mathbf{PF_6})_2$·DCE, were acquired in the solid-state (ATR; 4000-400 cm^{-1}; Figures S17 – S19). All compounds share vibrational patterns associated with the neutral L^0 ligand in the range 1670 – 1580 cm^{-1}, with the presence of ligands in different redox states in the neutral species accounting for the more complex spectra than their dicationic counterparts.[48,73] These observations are consistent with structural analysis that $\mathbf{1}^{2+}(\mathbf{PF_6})_2$·0.5DCE·0.5*i*Pr$_2$O and $\mathbf{3}^{2+}(\mathbf{PF_6})_2$·DCE exist as HS-Co^{II}-$(L^0)_3$ at 100 K with no $L^{\bullet-}$ present, and structural analysis of **1**·0.8EtOH, **2**, **3**·EtOH at 100 or 120 K that indicated a dominant HS-Co^{II}-$(L^{\bullet-})_2(L^0)$ state in the solid-state, which would give rise to both Ar-BIAN^0 and Ar-BIAN$^{\bullet-}$. For the neutral compounds, the ν(C=N) bands shift toward higher energies in the order **3** < **1** < **2** following the inductive effects of the ligand substituent. To improve the resolution in the region of interest for C−N stretches of α-diimine (1800–1550 cm^{-1}), solution state (CH_2Cl_2) infrared spectra were recorded (Figure S20). Good agreement in the region of interest is observed when comparing solid and solution-state measurements for all compounds.

Magnetic Measurements

Variable temperature magnetic susceptibility measurements were conducted for $\mathbf{1}^{2+}(\mathbf{PF_6})_2$·0.5DCE·0.5*i*Pr$_2$O, $\mathbf{3}^{2+}(\mathbf{PF_6})_2$·0.6DCE, **1**·0.8EtOH, **2**, **3**·EtOH (Figure 4) between 1.85 and 300 K to further probe the electronic state adopted by each compound in the solid-state and the variation with temperature. Variable field magnetization measurements are presented in Figures S21 and S22. At 300 K, the thermal product of the molar magnetic susceptibility ($\chi_M T$)

values for both dicationic compounds $\mathbf{1}^{2+}(\mathbf{PF_6})_2$·0.5DCE·0.5iPr$_2$O and $\mathbf{3}^{2+}(\mathbf{PF_6})_2$·0.6DCE of 3.0 and 2.7 cm^3 K mol^{-1}, respectively, are consistent with a HS-Co^{II}-(L^0)$_3$ charge distribution. This is in agreement with the structural analysis at 100 K. The $\chi_M T$ values are much higher than the spin-only value for S = 3/2 with g = 2, indicating spin-orbit coupling contributions to the magnetic susceptibility, common for HS-Co^{II} in a distorted ligand field.[59] The $\chi_M T$ remains essentially constant until 100 K, after which it decreases more rapidly to reach 1.8 and 1.7 cm^3 K mol^{-1} at 1.85 K for $\mathbf{1}^{2+}(\mathbf{PF_6})_2$·0.5DCE·0.5iPr$_2$O and $\mathbf{3}^{2+}(\mathbf{PF_6})_2$·0.6DCE, respectively, due to depopulation of the HS-Co^{II} spin-orbit coupled states. The observed behavior discounts thermally-induced VT to the LS-Co^{III}-(L$^{\bullet-}$)(L^0)$_2$ state for both compounds.

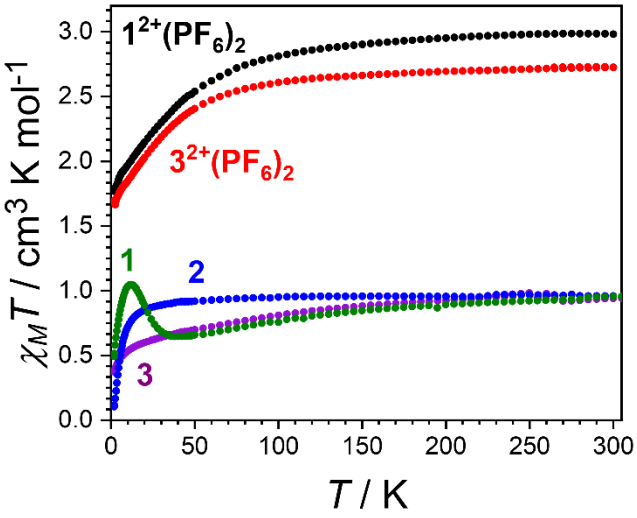

Figure 4. Temperature dependence of the χT product for $\mathbf{1}^{2+}(\mathbf{PF_6})_2$·0.5DCE·0.5iPr$_2$O (black), $\mathbf{3}^{2+}(\mathbf{PF_6})_2$·DCE (red), **1**·0.8EtOH (green), **2** (blue), and **3**·EtOH (purple) in the solid state at 0.1 T (χ, the dc magnetic susceptibility, is defined as M/H per mole of complex; M and H being the magnetization and applied magnetic field, respectively).

At 300 K, $\chi_M T$ values for the neutral compounds **1**·0.8EtOH, **2**, and **3**·EtOH are all approximately 0.95 $cm^3\,K\,mol^{-1}$, indicating a similar charge distribution (Figure 4). For **1**·0.8EtOH and **3**·EtOH, the $\chi_M T$ product decreases gradually below 200 K, whilst **2** remains approximately constant until 50 K. Below 50 K, the $\chi_M T$ response diverges for **1**·0.8EtOH compared to **2** and **3**·EtOH. For **1**·0.8EtOH, an increase is observed to reach a maximum of 1.1 $cm^3\,K\,mol^{-1}$ at 12 K, before rapidly decreasing to 0.49 $cm^3\,K\,mol^{-1}$ at 1.85 K. For **2** and **3**·EtOH, the $\chi_M T$ response below 50 K rapidly decreases to reach values of 0.10 and 0.37 $cm^3\,K\,mol^{-1}$, respectively, at 1.85 K. The low temperature feature exhibited by **1**·0.8EtOH is reminiscent of the onset of intermolecular interactions, which are perhaps mitigated in the case of **2** and **3**·EtOH due to differences in the coordinated ligands and the crystal lattice.

The ambient $\chi_M T$ values for the neutral compounds **1**·0.8EtOH, **2**, and **3**·EtOH are much lower than expected for a HS-Co^{II}-$(L^{\bullet-})_2(L^0)$ state, as suggested by structural analysis and IR, with negligible, or weak, magnetic exchange interactions. For example, the exchange in two HS-Co^{II}-semiquinonate complexes was determined to be weakly antiferromagnetic, with room temperature $\chi_M T$ values of 3.3 and 3.6 $cm^3\,K\,mol^{-1}$, consistent with uncoupled HS-Co^{II} and semiquinonate ligand.[74] Assignment of the electronic state of the three neutral compounds based on the magnetic behavior is much more complex in comparison with the dicationic equivalents, with competing strong $Co\cdots L^{\bullet-}$ and $L^{\bullet-}\cdots L^{\bullet-}$ exchange interactions expected from the DFT calculations (Table S5) for all electronic states, and a mix of the HS-Co^{II} and LS-Co^{II} charge distributions indicated in the structural analysis. Despite the experimentally observed $\chi_M T$ values being close to the theoretical value of 1.125 $cm^3\,K\,mol^{-1}$ for the LS-Co^{III}-$(L^{\bullet-})_3$ (Scheme 3) and HS-Co^{II}-$(L^{\bullet-})_2(L^0)$ states, these electromers are discounted based on structural analysis and IR, with support from

DFT. The behavior observed for **1**·0.8EtOH, **2**, and **3**·EtOH therefore arise from a HS-Co^{II}-$(L^{\bullet-})_2(L^0)$ state with substantial antiferromagnetic coupling between the HS-Co^{II} center and $L^{\bullet-}$ (calculated as –143 cm^{-1} for **1**, –76 cm^{-1} for **2**, –498 cm^{-1} for **3**) and between the two $L^{\bullet-}$ ligands (calculated as –128 cm^{-1} for **1**, –401 cm^{-1} for **2**, –30 cm^{-1} for **3**) (Scheme 3) as suggested by the DFT studies. These antiferromagnetic exchange interactions dominate, even at room temperature, resulting in the observed low $\chi_M T$.

Other compounds previously investigated for VT that feature more than one radical ligand coordinated to HS-Co^{II} have also exhibited lower than expected $\chi_M T$ responses, and although attempts have been made to justify this, an exact mechanism of exchange remains elusive.[33,75–77] Furthermore, related 3*d* and lanthanoid complexes coordinated to multiple Ar-BIAN$^{\bullet-}$ ligands display complex magnetic behavior.[36,38,69,78] These compounds exhibit strong antiferromagnetic metal$\cdots L^{\bullet-}$, and $L^{\bullet-}\cdots L^{\bullet-}$ exchange, with the competition between both modes of exchange and the trigonal symmetry of the system resulting in spin-frustration.[79] In the 3*d* metal cases, the spin-frustration was reported to give rise to multiple low-lying excited states, quenching the anisotropy of the metal, resulting in temperature-independent paramagnetism (TIP).[38,80,81]

In such spin systems as adopted by **1**, **2** and **3**, the behavior is undoubtedly challenging to model, and a conventional spin-only Hamiltonian is not appropriate. Certainly, there is more to be understood about magnetic exchange interactions in such compounds, but this falls outside of the scope of this study. One aspect that is clear is that for all measured compounds, the $\chi_M T$ remains relatively constant from 50-300 K, suggesting that neither a VT nor SCO interconversion occur in the solid-state. Rather, the HS-Co^{II}-L^0 containing electromer (HS-Co^{II}-$(L^0)_3$ for $\mathbf{1^{2+}(PF_6)_2}$ and $\mathbf{3^{2+}(PF_6)_2}$, and HS-Co^{II}-$(L^{\bullet-})_2(L^0)$ for **1**, **2** and **3)** is the ground-state in the solid-state. Although

the possibility of VT is suggested for **3** by gas phase DFT, the solid-state structural and magnetic data agree that the necessary LS-Co^{III}-$(L^{\bullet-})_3$ ground state is not observed.

Electronic Spectroscopy

In the solid-state, compounds $\mathbf{1^{2+}(PF_6)_2}$, $\mathbf{3^{2+}(PF_6)_2}$, **1**, **2** and **3** all exist in the HS-Co^{II}-L^0 containing electronic state at all measured temperatures. However, it is possible that a compound can exhibit a different electronic state in solution compared to the solid state,[33,82] which may be solvent dependent.[83] Electronic absorption spectra (Figure 5, Figures S23-S27, Table S10) were recorded for $\mathbf{1^{2+}(PF_6)_2}$, **1**, **2**, **3**, and $\mathbf{3^{2+}(PF_6)_2}$ in various solvents with a range of dielectric constants: MeCN (κ = 37.5), CH_2Cl_2 (κ = 8.93), tetrahydrofuran (THF) (κ = 7.58), and toluene (κ = 2.38) at room temperature. In MeCN and CH_2Cl_2, the visible region of the spectra of $\mathbf{1^{2+}(PF_6)_2}$ and $\mathbf{3^{2+}(PF_6)_2}$ is dominated by absorptions at approximately 25000 cm^{-1} arising from intra-ligand (IL) processes associated with the L^0 form of the Ar-BIAN ligand (Figure 5, Figures S23, S24).[48,84] The lack of features associated with Ar-$BIAN^{\bullet-}$ confirms a HS-Co^{II}-$(L^0)_3$ state in solution at room temperature for $\mathbf{1^{2+}(PF_6)_2}$ and $\mathbf{3^{2+}(PF_6)_2}$, as observed in the solid-state. Compound $\mathbf{1^{2+}(PF_6)_2}$ also features a very weak broad band centered at 10160 cm^{-1} in the NIR region, assigned as a $^4T_{1g} \rightarrow {}^4T_{2g}$ d-d transition; the analogous transition was difficult to discern from the baseline in the case of $\mathbf{3^{2+}(PF_6)_2}$.

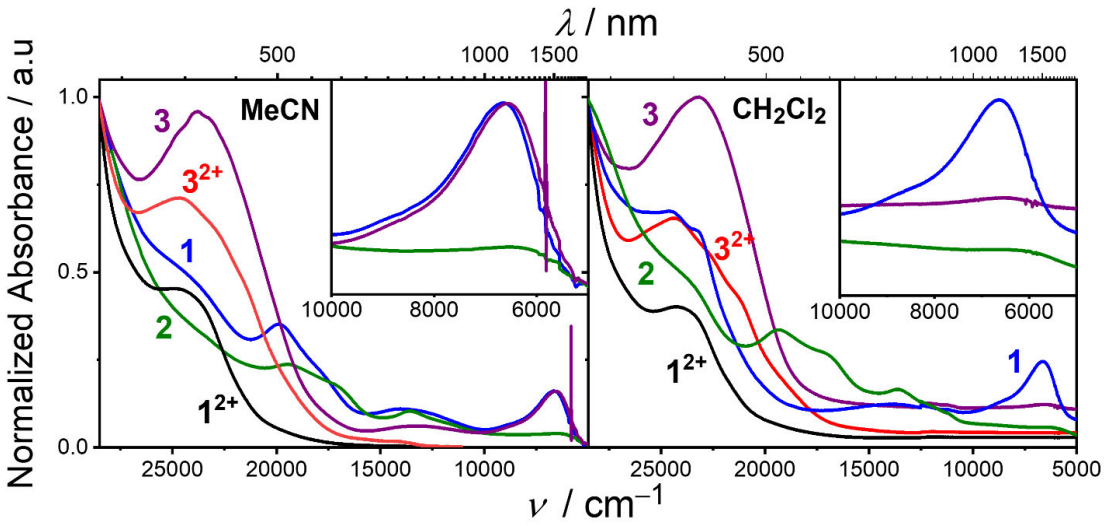

Figure 5. UV-Vis-NIR absorption spectra for MeCN solutions (left) and CH_2Cl_2 (right) for $\mathbf{1}^{2+}$ (black), $\mathbf{3}^{2+}$ (red), **1** (blue), **2** (green), and **3** (purple) at room temperature, with inset emphasizing the NIR region for **1**, **2** and **3**.

For **1**, **2** and **3**, multiple broad absorption features are observed across the visible region in the range of solvents (MeCN, CH_2Cl_2, THF, toluene). Anecdotally, an octahedral HS-Co(II) (d^7) ion displays more spin-allowed d-d transitions than LS-Co(III) (d^6), which is consistent with the broad range of low intensity, low energy absorption features of **1**, **2** and **3**. The dominant high-energy features arise from a combination of IL^0 (Ar-$BIAN^0$ intraligand transitions) and $IL^{\bullet-}$ transitions (Ar-$BIAN^{\bullet-}$ intraligand transitions) (Figure 5, Figures S25-S27).[48,84] The $IL^{\bullet-}$ transitions decrease in energy from **3** (23810 cm^{-1}), to **1** (19880 cm^{-1}) and **2** (19493 cm^{-1}), corresponding to the shift from electron-donating to electron-withdrawing groups on the Ar-BIAN ligand. At lower energies (13350–14250 cm^{-1}), ligand-to-metal charge transfer (LMCT) features are also observed for all three neutral compounds (Figure 5). The assignment of features confirms

that in solution at room temperature, **1**, **2** and **3** are present as HS-Co^{II}-$(L^{\bullet-})_2(L^0)$, mirroring the solid-state.

In MeCN, **1**, **2**, and **3** all feature a near infrared (NIR) band, assigned to a ligand-to-ligand intervalence charge transfer (IVCT) process involving the formally $L^{\bullet-}$ and L^0 ligand redox states.[36,38] This discounts a pure LS-Co^{III}-$(L^{\bullet-})_3$ state for the three compounds, further confirming the HS-Co^{II}-$(L^{\bullet-})_2(L^0)$ electronic state in solution at room temperature. The degree of electronic coupling between the Ar-BIAN ligands in **1**, **2**, and **3** can be described by the Robin and Day classification system (see Supporting Information),[85] and the electronic coupling parameter (H_{AB}) extracted from the energy and shape of the IVCT band in the framework of Marcus-Hush theory.[86]

Complex **1** in MeCN features an absorption envelope in the NIR region with an apparent maximum at 6645 cm^{-1}, which was deconvoluted by two Gaussian functions (Figure S28, Table S11) centered at ν_{max} = 6640(6) cm^{-1} with half-height width $\Delta\nu_{1/2}$ = 1441(3) cm^{-1} and at ν_{max} = 8400(90) cm^{-1} with $\Delta\nu_{1/2}$ = 3400(300) cm^{-1}. Similar low-energy absorption envelopes were also observed in MeCN for compounds **2** and **3** (Figures S29, S30, Table S11) and deconvoluted in each case to two-band patterns ν_{max} = 6050(20) cm^{-1} ($\Delta\nu_{1/2}$ = 1580(90) cm^{-1}) and ν_{max} = 7700(100) cm^{-1} ($\Delta\nu_{1/2}$ = 2900(700) cm^{-1}) for **2** and ν_{max} = 6520(6) cm^{-1} ($\nu_{1/2}$ = 1470(40) cm^{-1}) and ν_{max} = 8100(100) cm^{-1} ($\Delta\nu_{1/2}$ = 3200(300) cm^{-1}) for **3**. These absorption features proved to be solvent dependent, reducing in intensity in CH_2Cl_2, and undetected in THF and toluene, allowing for assignment of **1**, **2** and **3** to Class II. This indicates a localized electronic structure and solvent environment, and therefore the IVCT is linked to the reorganization energy, which in turn is linked to the energy of the optical charge transfer band. Marcus-Hush analysis of the lower energy band shape permits estimation of H_{AB} for each of these ligand mixed-valence complexes (**1**, 721 cm^{-1};

2, 790 cm^{-1}; and **3**, 736 cm^{-1} (Table S11). These values suggest similar weak electronic coupling and low levels of delocalization for **1**, **2** and **3**.[52,87]

Electrochemical and Spectroelectrochemical Studies

After establishing that in solution at room temperature compounds $\mathbf{1^{2+}(PF_6)_2}$ and $\mathbf{3^{2+}(PF_6)_2}$ adopt the HS-Co^{II}-$(L^0)_3$ state, and **1**, **2** and **3** are in the HS-Co^{II}-$(L^{\bullet-})_2(L^0)$ state, mirroring solid-state observations, electrochemical and spectroelectrochemical studies were conducted. Cyclic voltammograms of the (air-stable) dicationic complexes $\mathbf{1^{2+}(PF_6)_2}$ and $\mathbf{3^{2+}(PF_6)_2}$ in CH_2Cl_2, with resting potentials of −0.1 and −0.2 V respectively, reveal one oxidation process (*I*), assigned to the Co^{II}/Co^{III} redox couple, and four reduction processes (*II*, *III*, *IV* and *V*) associated with the consecutive one electron reduction of each L^0 to $L^{\bullet-}$ (*II – IV)* and further reduction of one $L^{\bullet-}$ to L^{2-} (*V*) within the measured potential range (Figure 6). In both cases, the first oxidation (*I*) and first reduction (*II*) were found to be electrochemically reversible (Figure S31, S32). Processes *III*, *IV* and *V* are completely irreversible. After the reduction *III*, partial decomposition was detected electrochemically even while recording the voltammograms at higher scan rates, with an additional redox species with potential near process *II* becoming prominent as a result. As expected for the HS-Co^{II}-$(L^0)_3$ state adopted in solution at room temperature by $\mathbf{1^{2+}(PF_6)_2}$ and $\mathbf{3^{2+}(PF_6)_2}$, only ligand-based reductions (no oxidations) and cobalt based oxidation are observed.

Static voltammograms were measured for the isolated neutral compounds **1**, **2** and **3** under analogous conditions to the dicationic compounds $\mathbf{1^{2+}(PF_6)_2}$ and $\mathbf{3^{2+}(PF_6)_2}$ (Figures S33, S34). The five processes identified in the neutral compounds **1** and **3** are at the same positions as their dicationic analogues, as expected for redox products. The resting potential of −1.2, −0.9, and −1.3

V for **1**, **2** and **3**, respectively, indicate that now process *II* and *III* are oxidations, consistent with the established HS-Co^{II}-$(L^{\bullet-})_2(L^0)$ electronic state in solution at room temperature.

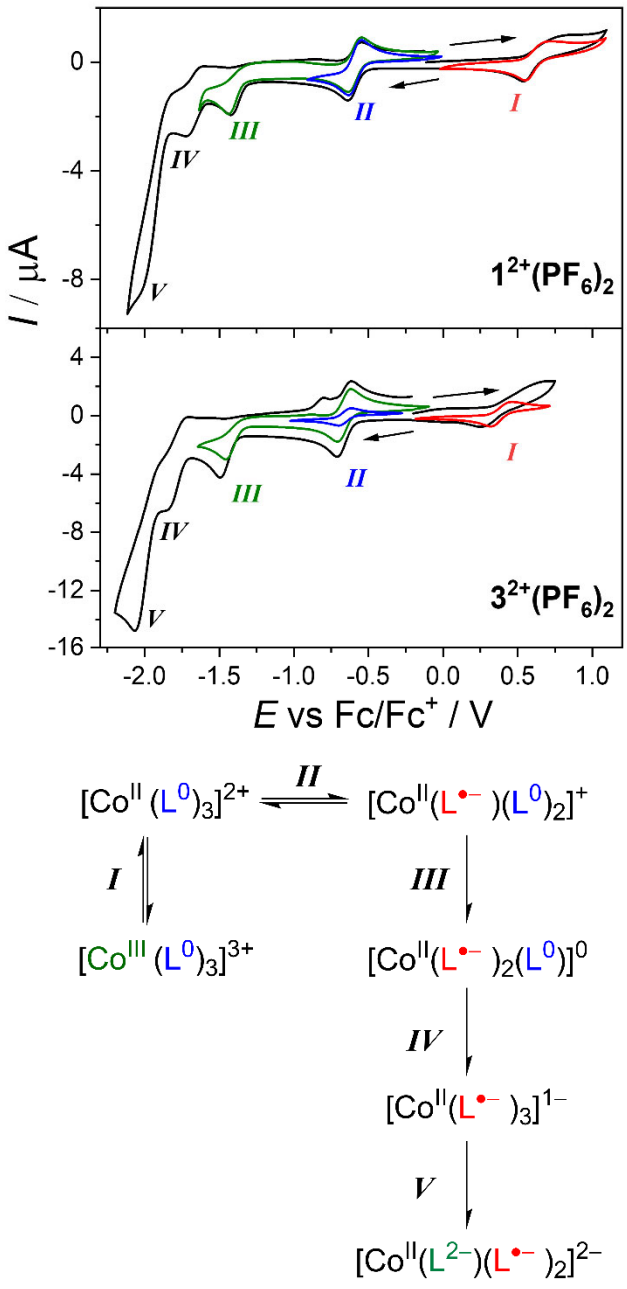

Figure 6. Cyclic voltammograms (0.1 M NBu_4PF_6 / CH_2Cl_2) of $\mathbf{1^{2+}(PF_6)_2}$ and $\mathbf{3^{2+}(PF_6)_2}$ at scan rate of 100 mV/s (top). The colored lines plot the voltammograms measured with a switching

potential immediately past the first oxidation (red), first reduction (blue), second reduction (green). Assignments of redox processes and associated species (bottom).

Guided by the UV-Vis-NIR spectra and electrochemical results, the reversible oxidation (*I*) and first reduction (*II*) processes of $\mathbf{1^{2+}(PF_6)_2}$ and $\mathbf{3^{2+}(PF_6)_2}$ were studied by UV-Vis-NIR spectroelectrochemical methods in CH_2Cl_2. Upon oxidation of $Co^{II} \rightarrow Co^{III}$ for both compounds, all spectral features grow in intensity and shift toward lower energies. An isosbestic point is observed in the higher energy region (ca 33300 cm^{-1}), and corresponds to the red shift of the high energy π^* orbitals of the ligands, presumably through charge effects.[48] The lower energy absorbances are all very similar between the Co^{II} species and the oxidised Co^{III} form, but with increased intensities for the Co^{III} containing species.

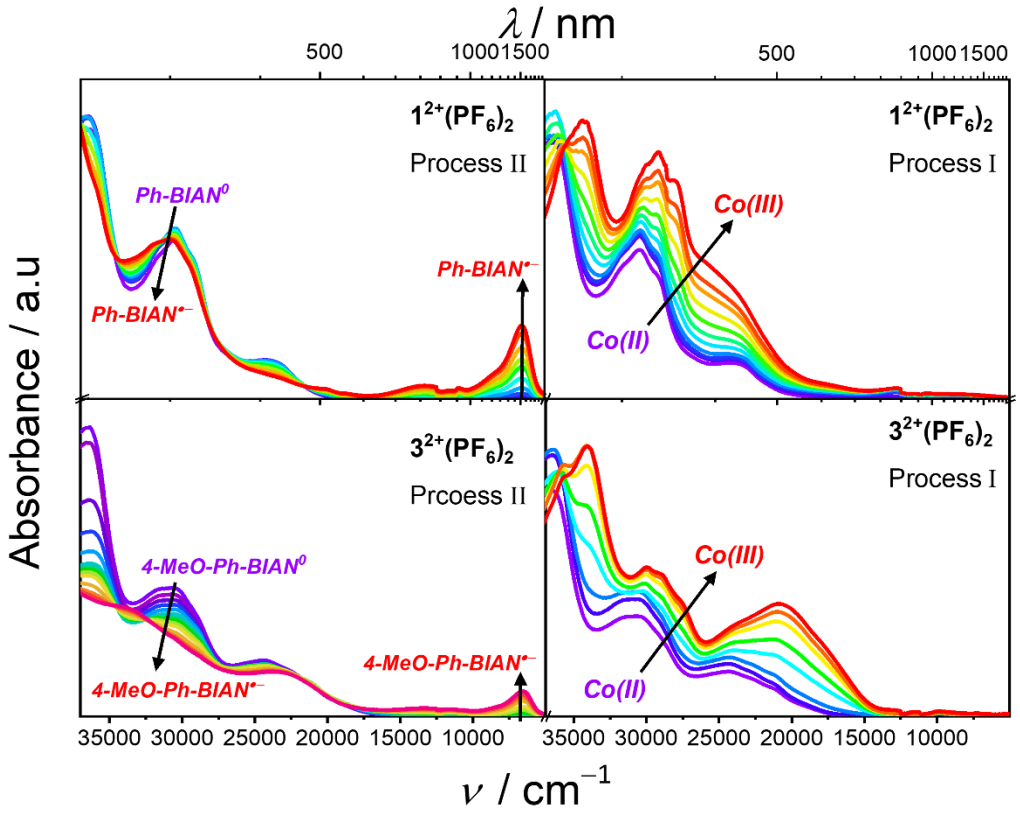

Figure 7. Spectroelectrochemical data (UV-Vis-NIR) for the 1st reduction (left) and 1st oxidation (right) of complexes $\mathbf{1^{2+}(PF_6)_2}$ and $\mathbf{3^{2+}(PF_6)_2}$ measured in 0.1 M solution of NBu_4PF_6 in CH_2Cl_2. The 1st reduction is associated with $L^0 \rightarrow L^{\bullet-}$ (process *II*) and the 1st oxidation is associated with $Co^{II} \rightarrow Co^{III}$ redox couple (process *I*).

Upon reduction of $\mathbf{1^{2+}(PF_6)_2}$ and $\mathbf{3^{2+}(PF_6)_2}$ through process *II*, a clear isosbestic point is observed in the visible region (21400 cm^{-1} for $\mathbf{1^{2+}(PF_6)_2}$ and 19500 cm^{-1} for $\mathbf{3^{2+}(PF_6)_2}$), with features between 36000-24000 cm^{-1} (277–416 nm) that arise from the formation of the reduced form of the ligand, $L^{\bullet-}$, giving rise to the electronic state HS-Co^{II}-($L^{\bullet-}$)(L^0)$_2$ (analogous to $\mathbf{1^+(PF_6)}$). An additional absorbance in the visible region that appears at 13330 cm^{-1} (750 nm) for $\mathbf{1^{2+}(PF_6)_2}$

and 13100 cm^{-1} (763 nm) for $\mathbf{3^{2+}(PF_6)_2}$ has not been observed in the spectrum of free Ph-BIAN$^{\bullet-}$ or 4-MeO-Ph-BIAN$^{\bullet-}$,[84] discounting an IL$^{\bullet-}$ transition, and is likely the an LMCT transition. The observed features resemble those present in the spectra for **1**, **2** and **3**. Most interestingly, a peak emerges in the NIR region of the spectrum for both compounds ($\mathbf{1^+}$, 6630 cm^{-1} (1508 nm); $\mathbf{3^+}$, 6600 cm^{-1} (1515 nm)) characteristic of the IVCT process arising from the presence of Ar-BIAN in different redox states ($L^0/L^{\bullet-}$), as observed for **1**, **2** and **3**. Fitting the NIR peaks Figures S35, S36) produced upon cycling through process *II* to give the resulting monocationic ($\mathbf{1^+}$ and $\mathbf{3^+}$) complex gave ν_{max} = 6610(2) cm^{-1} ($\Delta\nu_{1/2}$ = 1310(10) cm^{-1}) and ν_{max} = 7930(30) cm^{-1} ($\Delta\nu_{1/2}$ = 2830(70) cm^{-1}) for $\mathbf{1^+}$, and ν_{max} = 6552(2) cm^{-1} ($\Delta\nu_{1/2}$ = 1350(10) cm^{-1}) and ν_{max} = 79730(50) cm^{-1} ($\Delta\nu_{1/2}$ = 3000(100) cm^{-1}) for $\mathbf{3^+}$. The H_{AB} of the lower energy band of 655 and 675 cm^{-1} for $\mathbf{1^+}$ and $\mathbf{3^+}$, respectively, indicate that like **1**, **2** and **3** an MV Class II is likely for both cases.

Variable Temperature Electronic Spectroscopy

The electronic state of **1**, **2** and **3** in solution at room temperature has been established as HS-Co^{II}-$(L^{\bullet-})_2(L^0)$ via electronic absorption spectroscopy, electrochemistry and spectroelectrochemistry. This mirrors the solid-state observations. However, DFT calculations (*vide supra*) for **3** point to a LS-Co^{III}-$(L^{\bullet-})_3$ ground state and the possibility of thermally-induced VT (Scheme 2). No evidence of VT was observed in the solid state. However, as mentioned, VT can still occur in solution even if not observed in the solid.[33] In order to investigate the possibility in solution, lower temperature absorption spectra were measured for both **1** and **3** upon cooling down to our instrumental limit of 243 K in both CH_2Cl_2 and MeCN (Figure 8 and Figures S37, S38).

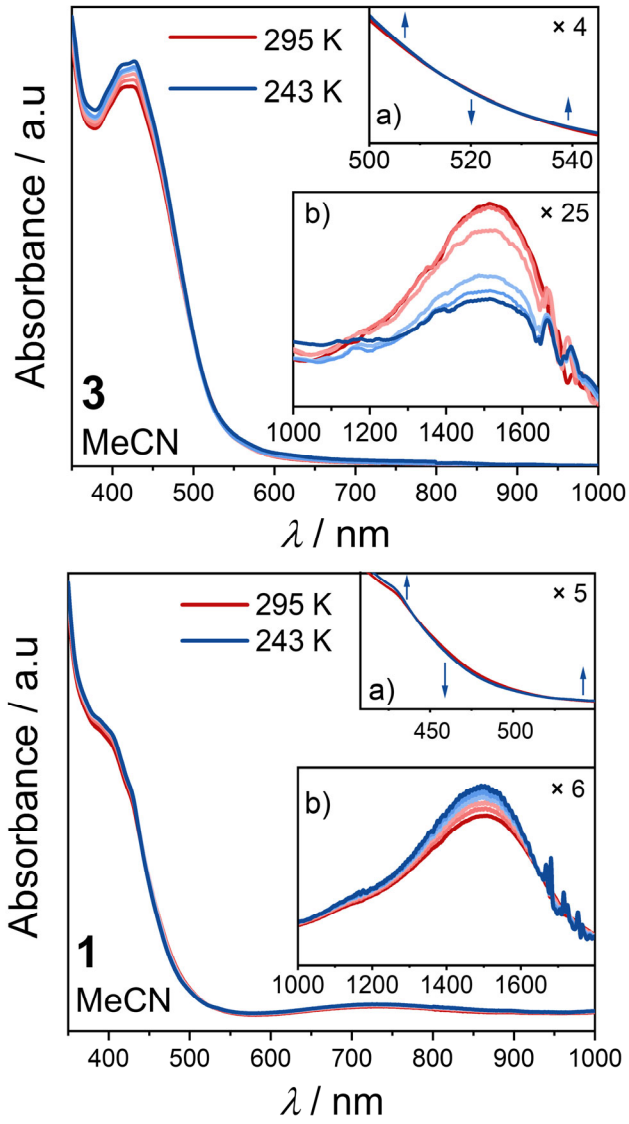

Figure 8. Variable temperature UV-Vis-NIR absorption spectra for **3** (top) and **1** (bottom) in MeCN between 243 and 295 K, with inset (a) highlighting isosbestic points and (b) the temperature dependence of the IVCT band in the NIR region.

For **3** in CH_2Cl_2, only minimal changes are evident in the visible range upon cooling, including a slight increase in the $IL^{\bullet-}$ band intensity at 430 nm (23200 cm^{-1}), but the IVCT peak

exhibits little change, consistent with no VT (Figure S37). However, in MeCN, a more significant increase is evident in intensity of the $IL^{\bullet-}$ transition at 430 nm, with two closely spaced isosbestic point at 513 and 522 nm, indicating the onset of an equilibrium between two (or more) species (Figure 8). These isosbestic points are found at a similar energy to that observed in the spectroelectrochemical measurements on cycling through reduction process *II*. More intriguingly, on cooling, the IVCT band at ~1510 nm (6623 cm^{-1}) decreases significantly in intensity, indicating a decrease in the mixed-valent character of the ligands, suggestive of increased LS-Co^{III}-$(L^{\bullet-})_3$ population. This change is reversed upon warming to room temperature, indicating a reversible thermal process (Figure S39). Similar changes in IVCT band intensities with temperature have been instrumental for monitoring thermally-induced VT for cobalt complexes involving interconversion from two semiquinonate ligands to one semiquinonate and one catecholate ligand.[44,88–90] Therefore, the variable temperature data suggests thermally-induced VT for **3** in MeCN, involving interconversion between LS-Co^{III}-$(L^{\bullet-})_3$ at low temperature and HS-Co^{III}-$(L^{\bullet-})_2(L^0)$ at higher temperature (Scheme 3). This is consistent with DFT predictions. The observed effect of solvent on the VT transition is consistent with previous observations for cobalt-dioxolene systems, where solvent is known to alter the relative stability of the different charge distributions and modulate the charge transfer processes.[83] Specifically, chlorinated solvents tend to stabilize the HS-Co^{II}-semiquinonate state, whereas nitrile solvents stabilize the LS-Co^{III}-catecholate tautomer.[19,43] For comparison, compound **1** was also measured down to 243 K in CH_2Cl_2 and MeCN. In both solvents, the $IL^{\bullet-}$ bands around 395 nm (25320 cm^{-1}) decrease very slightly with decreasing temperature, with isosbestic points around 437 and 522 nm. However, the IVCT band increases slightly in intensity upon cooling, rather than decreases, indicating no VT transition for this compound.

CONCLUSIONS

The $[Co(Ar\text{-}BIAN)_3]^{n+}$ (n = 0, 1, 2) family of homoleptic cobalt complexes incorporating an electronically diverse range of α-diimine Ar-BIAN ligands have been synthesized and their electronic structures analyzed via a combination of computational, structural, magnetic, spectroscopic and electrochemical techniques. The aim of this work at the outset was to explore the possibility of molecular switchability in the form of thermally-induced SCO or valence VT. Density functional theory calculations proved invaluable in guiding the choice of compounds to synthesize and investigate experimentally, with the critical DFT output being the relative energies of the electromeric forms relevant for the different types of interconversions. The DFT calculations of all members of the $[Co(Ar\text{-}BIAN)_3]^{n+}$ family complexes studied here suggested that SCO is likely unattainable for this family. This can be attributed to the inability of the Ar-BIAN / Ar-BIAN$^{\bullet-}$ ligands to provide a sufficiently strong ligand field to stabilize a LS-Co^{II} containing electromer. In contrast, the calculations suggested that a neutral $[Co(Ar\text{-}BIAN)_3]$ complex with a strongly electron-donating Ar-BIAN / Ar-BIAN$^{\bullet-}$ ligand combination might afford VT by stabilizing the LS-Co^{III}-$(L^{\bullet-})_3$ ground state and allowing interconversion to a low-lying HS-Co^{II}-$(L^{\bullet-})_2(L^0)$ state upon heating. The most promising candidate compound for VT was thus identified as $[Co(4\text{-}MeO\text{-}Ph\text{-}BIAN)_3]$.

Six members of the $[Co(Ar\text{-}BIAN)_3]^{n+}$ (n = 0, 1, 2) family with three different Ar-BIAN ligands were synthesized and characterized in the solid state and solution. Solid state structural and magnetic data are consistent with a HS-Co^{II}-L^0 containing electronic structure for all six complexes, with no VT processes evident in the solid state. Detailed electronic absorption spectroscopy, electrochemistry and spectroelectrochemistry studies performed on several analogues in solution *at room temperature* are consistent with the ground state charge distributions

observed in the solid state. However, variable temperature electronic absorption spectra of [Co(4-MeO-Ph-BIAN)$_3$] in MeCN show evidence of a valence tautomeric interconversion from the HS-Co^{II}-(L$^{\bullet-}$)$_2$(L^0) state at room temperature to LS-Co^{III}-(L$^{\bullet-}$)$_3$ upon cooling to 243 K. Specifically, the ligand-based IVCT band in the NIR decreases significantly in intensity upon cooling, consistent with a decrease in the extent of ligand mixed-valency as HS-Co^{II}-(L$^{\bullet-}$)$_2$(L^0) interconverts to LS-Co^{III}-(L$^{\bullet-}$)$_3$. Although the extent of the interconversion cannot be determined with the present data, the DFT prediction of thermally-induced VT for [Co(4-MeO-Ph-BIAN)$_3$] has been experimentally verified. This study has thus identified a new chemical family of valence tautomeric complexes. Furthermore, this work has demonstrated that maximization of ligand electron donation via simultaneously maximizing the negative charge on the ligands, and incorporating electron-donating substituents, sufficiently stabilizes the LS-Co^{III} containing tautomer, which is key for accessing VT in this [Co(Ar-BIAN)$_3$]$^{n+}$ (n = 0, 1, 2) family of complexes. Although beyond the scope of this work, it is conceivable then that extending this principle by incorporating the dianionic Ar-BIAN^{2-} ligands might facilitate the alternative VT interconversion possible with these ligands: LS-Co^{III}-(L^{2-}) ⇌ HS-Co^{II}-(L$^{\bullet-}$), rather than the LS-Co^{III}-(L$^{\bullet-}$) ⇌ HS-Co^{II}-(L^0) observed for [Co(4-MeO-Ph-BIAN)$_3$]. Most importantly, this study clearly indicates the power of DFT-guided selection of candidate compounds for the efficient development of new functional molecules.

ASSOCIATED CONTENT

Supporting Information

The Supporting Information is available free of charge at X.

Details of synthetic, experimental and theoretical methods, structure refinement details, DFT, TGA, IR, crystallography, PXRD, magnetic measurements, UV-Vis-NIR, mixed-valency analysis, electrochemistry, and variable temperature UV-Vis-NIR (PDF).

DFT optimized XYZ coordinates of complexes (ZIP)

Accession Codes

CCDC 2178597− 2178602 contain the supplementary crystallographic data for this paper. These data can be obtained free of charge via www.ccdc.cam.ac.uk/data_request/cif, or by emailing data_request@ccdc.cam.ac.uk, or by contacting The Cambridge Crystallographic Data Centre, 12 Union Road, Cambridge CB2 1EZ, UK; fax: +44 1223 336033.

AUTHOR INFORMATION

Corresponding Author

Colette Boskovic − School of Chemistry, University of Melbourne, Victoria 3010, Australia; orcid.org/0000-0002-1882-2139; Email: c.boskovic@unimelb.edu.au

Author Contributions

[$] M. A. H. and J. T. J. contributed equally to this manuscript. The manuscript was written through contributions of all authors. All authors have given approval to the final version of the manuscript.

Notes

The authors declare no competing financial interest.

ACKNOWLEDGMENTS

C.B. thanks the Australian Research Council for financial support (DP190100854 and DP220100398). This research was undertaken in part using the MX1 and MX2 beamline at the Australian Synchrotron, part of ANSTO, Australia. A. A. S. thanks the Ministry of Science and Higher Education of the Russian Federation (State assignment in the field of scientific activity, project no. 0852-2020-0031). We are thankful to the University of Bordeaux, the Région Nouvelle Aquitaine, Quantum Matter Bordeaux (QMBx), the Centre National de la Recherche Scientifique (CNRS), and the Association Française de Magnétisme Moléculaire. We thank Prof. Keith Murray, Dr Wasinee Phonsri, and Maja Dunstan for preliminary magnetic measurements.

REFERENCES

(1) Aviram, A.; Ratner, M. A. Molecular Rectifiers. *Chem. Phys. Lett.* **1974**, *29*, 277–283.

(2) Markov, I. L. Limits on Fundamental Limits to Computation. *Nature* **2014**, *512*, 147–154.

(3) Xiang, D.; Wang, X.; Jia, C.; Lee, T.; Guo, X. Molecular-Scale Electronics: From Concept to Function. *Chem. Rev.* **2016**, 116, 4318–4440.

(4) Wasielewski, M. R.; Forbes, M. D. E.; Frank, N. L.; Kowalski, K.; Scholes, G. D.; Yuen-Zhou, J.; Baldo, M. A.; Freedman, D. E.; Goldsmith, R. H.; Goodson, T.; Kirk, M. L.; McCusker, J. K.; Ogilvie, J. P.; Shultz, D. A.; Stoll, S.; Whaley, K. B. Exploiting Chemistry and Molecular Systems for Quantum Information Science. *Nat. Rev. Chem.* **2020**, *4*, 490–504.

(5) Lefter, C.; Davesne, V.; Salmon, L.; Molnár, G.; Demont, P.; Rotaru, A.; Bousseksou, A. Charge Transport and Electrical Properties of Spin Crossover Materials: Towards Nanoelectronic and Spintronic Devices. *Magnetochemistry* **2016**, *2*, 18.

(6) Hao, G.; Cheng, R.; Dowben, P. A. The Emergence of the Local Moment Molecular Spin Transistor. *J. Phys. Condens. Matter* **2020**, *32*, 234002.

(7) Cornia, A.; Seneor, P. Spintronics: The Molecular Way. *Nat. Mater.* **2017**, *16*, 505–506.

(8) Yu, C. J.; Von Kugelgen, S.; Laorenza, D. W.; Freedman, D. E. A Molecular Approach to Quantum Sensing. *ACS Cent. Sci.* **2021**, *7*, 712–723.

(9) Paquette, M. M.; Plaul, D.; Kurimoto, A.; Patrick, B. O.; Frank, N. L.; Patrick, B. O. Opto-Spintronics: Photoisomerization-Induced Spin State Switching at 300 K in Photochrome Cobalt-Dioxolene Thin Films. *J. Am. Chem. Soc.* **2018**, *140*, 14990–15000.

(10) Senthil Kumar, K.; Ruben, M. Emerging Trends in Spin Crossover (SCO) Based Functional Materials and Devices. *Coord. Chem. Rev.* **2017**, *346*, 176–205.

(11) Urdampilleta, M.; Ayela, C.; Ducrot, P. H.; Rosario-Amorin, D.; Mondal, A.; Rouzières, M.; Dechambenoit, P.; Mathonière, C.; Mathieu, F.; Dufour, I.; Clérac, R. Molecule-Based Microelectromechanical Sensors. *Sci. Rep.* **2018**, *8*, 1–6.

(12) Karuppannan, S. K.; Martín-Rodríguez, A.; Ruiz, E.; Harding, P.; Harding, D. J.; Yu, X.; Tadich, A.; Cowie, B.; Qi, D.; Nijhuis, C. A. Room Temperature Conductance Switching in a Molecular Iron(Iii) Spin Crossover Junction. *Chem. Sci.* **2021**, *12*, 2381–2388.

(13) Sato, O.; Tao, J.; Zhang, Y.-Z. Control of Magnetic Properties through External Stimuli. *Angew. Chem., Int. Ed.* **2007**, *46*, 2152–2187.

(14) Kumar, K. S.; Ruben, M. Sublimable Spin-Crossover Complexes: From Spin-State Switching to Molecular Devices. *Angew. Chem., Int. Ed.* **2021**, *60*, 7502–7521.

(15) Hay, M. A.; Boskovic, C. Lanthanoid Complexes as Molecular Materials: The Redox Approach. *Chem. - Eur. J.* **2020**, 3608–3637.

(16) Gransbury, G. K.; Boskovic, C. Valence Tautomerism in D-Block Complexes. In *Encyclopedia of Inorganic and Bioinorganic Chemistry*; Wiley, 2021; pp 1–24.

(17) Hayami, S.; Holmes, S. M.; Halcrow, M. A. Spin-State Switches in Molecular Materials Chemistry. *J. Mater. Chem. C* **2015**, *3*, 7775–7778.

(18) Halcrow, M. A. *Spin-Crossover Materials: Properties and Applications*; John Wiley & Sons Ltd.; 2013

(19) Tezgerevska, T.; Alley, K. G.; Boskovic, C. Valence Tautomerism in Metal Complexes: Stimulated and Reversible Intramolecular Electron Transfer between Metal Centers and Organic Ligands. *Coord. Chem. Rev.* **2014**, *268*, 23–40.

(20) Droghetti, A.; Sanvito, S. Electric Field Control of Valence Tautomeric Interconversion in Cobalt Dioxolene. *Phys. Rev. Lett.* **2011**, *107* 047201.

(21) Li, B.; Zhao, Y. M.; Kirchon, A.; Pang, J. D.; Yang, X. Y.; Zhuang, G. L.; Zhou, H. C. Unconventional Method for Fabricating Valence Tautomeric Materials: Integrating Redox Center within a Metal-Organic Framework. *J. Am. Chem. Soc.* **2019**, *141*, 6822–6826.

(22) Vázquez-Mera, N. A.; Roscini, C.; Hernando, J.; Ruiz-Molina, D. Liquid-Filled Valence Tautomeric Microcapsules: A Solid Material with Solution-Like Behavior. *Adv. Funct. Mater.* **2015**, *25*, 4129–4134.

(23) Vázquez-Mera, N. A.; Novio, F.; Roscini, C.; Bellacanzone, C.; Guardingo, M.; Hernando, J.; Ruiz-Molina, D. Switchable Colloids, Thin-Films and Interphases Based on Metal

Complexes with Non-Innocent Ligands: The Case of Valence Tautomerism and Their Applications. *J. Mater. Chem. C* **2016**, *4*, 5879–5889.

(24) Tezgerevska, T.; Rousset, E.; Gable, R. W.; Jameson, G. N. L.; Sañudo, E. C.; Starikova, A.; Boskovic, C. Valence Tautomerism and Spin Crossover in Pyridinophane–Cobalt–Dioxolene Complexes: An Experimental and Computational Study. *Dalton Trans.* **2019**, *48*, 11674–11689.

(25) Drath, O.; Boskovic, C. Switchable Cobalt Coordination Polymers: Spin Crossover and Valence Tautomerism. *Coord. Chem. Rev.* **2018**, *375*, 256–266.

(26) Goodwin, H. A. Spin Crossover in Cobalt(II) Systems. In *Spin Crossover in Transition Metal Compounds II*; Springer Berlin Heidelberg: Berlin, Heidelberg: Cambridge, 2012; Vol. 234, pp 23–47.

(27) Krivokapic, I.; Zerara, M.; Daku, M. L.; Vargas, A.; Enachescu, C.; Ambrus, C.; Tregenna-Piggott, P.; Amstutz, N.; Krausz, E.; Hauser, A. Spin-Crossover in Cobalt(II) Imine Complexes. *Coord. Chem. Rev.* **2007**, *251*, 364–378.

(28) Kilner, C. A.; Halcrow, M. A. An Unusual Discontinuity in the Thermal Spin Transition in $[Co(terpy)_2][BF_4]_2$ *Dalton Trans.* **2010**, *39*, 9008–9012.

(29) Hayami, S.; Komatsu, Y.; Shimizu, T.; Kamihata, H.; Lee, Y. H. Spin-Crossover in Cobalt(II) Compounds Containing Terpyridine and Its Derivatives. *Coord. Chem. Rev.* **2011**, *255*, 1981–1990.

(30) Kobayashi, F.; Komatsumaru, Y.; Akiyoshi, R.; Nakamura, M.; Zhang, Y.; Lindoy, L. F.; Hayami, S. Water Molecule-Induced Reversible Magnetic Switching in a Bis-Terpyridine

Cobalt(II) Complex Exhibiting Coexistence of Spin Crossover and Orbital Transition Behaviors. *Inorg. Chem.* **2020**, *59*, 16843–16852.

(31) Cowan, M. G.; Olguín, J.; Narayanaswamy, S.; Tallon, J. L.; Brooker, S. Reversible Switching of a Cobalt Complex by Thermal, Pressure, and Electrochemical Stimuli: Abrupt, Complete, Hysteretic Spin Crossover. *J. Am. Chem. Soc.* **2012**, *134*, 2892–2894.

(32) Yang, C.; Nikiforidis, G.; Park, J. Y.; Choi, J.; Luo, Y.; Zhang, L.; Wang, S. C.; Chan, Y. T.; Lim, J.; Hou, Z.; Baik, M. H.; Lee, Y.; Byon, H. R. Designing Redox-Stable Cobalt–Polypyridyl Complexes for Redox Flow Batteries: Spin-Crossover Delocalizes Excess Charge. *Adv. Energy Mater.* **2018**, *8*, 1702897.

(33) Fleming, C.; Chung, D.; Ponce, S.; Brook, D. J. R.; DaRos, J.; Das, R.; Ozarowski, A.; Stoian, S. A. Valence Tautomerism in a Cobalt-Verdazyl Coordination Compound. *Chem. Commun.* **2020**, *56*, 4400–4403.

(34) Bonanno, N. M.; Watts, Z.; Mauws, C.; Patrick, B. O.; Wiebe, C. R.; Shibano, Y.; Sugisaki, K.; Matsuoka, H.; Shiomi, D.; Sato, K.; Takui, T.; Lemaire, M. T. Valence Tautomerism in a [2 × 2] Co_4 Grid Complex Containing a Ditopic Arylazo Ligand. *Chem. Commun.* **2021**, *57*, 6213–6216.

(35) Wang, J.; Soo, H. Sen; Garcia, F. Synthesis, Properties, and Catalysis of p-Block Complexes Supported by Bis(Arylimino)Acenaphthene Ligands. *Commun. Chem.* **2020**, *3*, 1–13.

(36) Clark, K. M.; Bendix, J.; Clark, K. M. Delocalization and Valence Tautomerism in Vanadium Tris(Iminosemiquinone) Complexes. *Angew. Chem., Int. Ed.* **2016**, *55*, 2748–2752.

(37) Fedushkin, I. L.; Maslova, O. V.; Morozov, A. G.; Dechert, S.; Demeshko, S.; Meyer, F. Genuine Redox Isomerism in a Rare-Earth-Metal Complex. *Angew. Chem., Int. Ed.* **2012**, *51*, 10584–10587.

(38) Clark, K. M.; Bendix, J.; Heyduk, A. F.; Ziller, J. W. Synthesis and Characterization of a Neutral Titanium Tris(Iminosemiquinone) Complex Featuring Redox-Active Ligands. *Inorg. Chem.* **2012**, *51*, 7457–7459.

(39) Hill, N. J.; Vargas-Baca, I.; Cowley, A. H. Recent Developments in the Coordination Chemistry of Bis(Imino)Acenaphthene (BIAN) Ligands with s- and p-Block Elements. *Dalton Trans.* **2009**, *9226*, 240–253.

(40) Fedushkin, I. L.; Skatova, A. A.; Chudakova, V. A.; Fukin, G. K. Four-Step Reduction of Dpp-Bian with Sodium Metal: Crystal Structures of the Sodium Salts of the Mono-, Di-, Tri- and Tetraanions of Dpp-Bian. *Angew. Chem., Int. Ed.* **2003**, *42*, 3294–3298.

(41) Gasperini, M.; Ragaini, F.; Cenini, S. Synthesis of Ar-BIAN Ligands (Ar-BIAN = Bis(Aryl)Acenaphthenequinonediimine) Having Strong Electron-Withdrawing Substituents on the Aryl Rings and Their Relative Coordination Strength toward Palladium(0) and (II) Complexes. *Organometallics* **2002**, *21*, 2950–2957.

(42) Beni, A.; Dei, A.; Laschi, S.; Rizzitano, M.; Sorace, L. Tuning the Charge Distribution and Photoswitchable Properties of Cobalt–Dioxolene Complexes by Using Molecular Techniques. *Chem. - Eur. J.* **2008**, *14*, 1804–1813.

(43) Gransbury, G. K.; Boulon, M. E.; Petrie, S.; Gable, R. W.; Mulder, R. J.; Sorace, L.; Stranger, R.; Boskovic, C. DFT Prediction and Experimental Investigation of Valence

Tautomerism in Cobalt-Dioxolene Complexes. *Inorg. Chem.* **2019**, *58*, 4230–4243.

(44) Janetzki, J. T.; Zahir, F. Z. M.; Gable, R. W.; Phonsri, W.; Murray, K. S.; Goerigk, L.; Boskovic, C. A Convenient DFT-Based Strategy for Predicting Transition Temperatures of Valence Tautomeric Molecular Switches. *Inorg. Chem.* **2021**, *60*, 14475–14487.

(45) Schmitz, M.; Seibel, M.; Kelm, H.; Demeshko, S.; Meyer, F.; Krüger, H.-J. How Does a Coordinated Radical Ligand Affect the Spin Crossover Properties in an Octahedral Iron(II) Complex? *Angew. Chem., Int. Ed.* **2014**, *53*, 5988–5992.

(46) Fedushkin, I. L.; Maslova, O. V.; Baranov, E. V.; Shavyrin, A. S. Redox Isomerism in the Lanthanide Complex [(Dpp-Bian)Yb(DME)(μ-Br)]$_2$(Dpp-Bian = 1,2-Bis[(2,6-Diisopropylphenyl)Imino]Acenaphthene). *Inorg. Chem.* **2009**, *48*, 2355–2357.

(47) Starikov, A. G.; Starikova, A. A.; Minkin, V. I. Quantum Chemical Study of the Adducts of Azomethine Cobalt Complexes with Acenaphthene-1,2-Diimines. *Russ. J. Gen. Chem.* **2017**, *87*, 104–112.

(48) Nadurata, V. L.; Hay, M. A.; Janetzki, J. T.; Gransbury, G. K.; Boskovic, C. Rich Redox-Activity and Solvatochromism in a Family of Heteroleptic Cobalt Complexes. *Dalton Trans.* **2021**, *50*, 16631–16646.

(49) Tao, J.; Perdew, J. P.; Staroverov, V. N.; Scuseria, G. E. Climbing the Density Functional Ladder: Nonempirical Meta–Generalized Gradient Approximation Designed for Molecules and Solids. *Phys. Rev. Lett.* **2003**, *91*, 146401.

(50) Staroverov, V. N.; Scuseria, G. E.; Tao, J.; Perdew, J. P. Comparative Assessment of a New Nonempirical Density Functional: Molecules and Hydrogen-Bonded Complexes. *J. Chem.*

Phys. **2003**, *119*, 12129–12137.

(51) Frisch, M. J.; Trucks, G. W.; Schlegel, H. B.; Scuseria, G. E.; Robb, M. A.; Cheeseman, J. R.; Scalmani, G.; Barone, V.; Petersson, G. A.; Nakatsuji, H.; Li, X.; Caricato, M.; Marenich, A. V.; Bloino, J.; Janesko, B. G.; Gomperts, R.; Mennucci, B.; Hratch, D. J. Gaussian 16 Rev. C.01.

(52) Gransbury, G. K.; Livesay, B. N.; Janetzki, J. T.; Hay, M. A.; Gable, R. W.; Shores, M. P.; Starikova, A.; Boskovic, C. Understanding the Origin of One- or Two-Step Valence Tautomeric Transitions in Bis(Dioxolene)-Bridged Dinuclear Cobalt Complexes. *J. Am. Chem. Soc.* **2020**, *142*, 10692–10704.

(53) Minkin, V. I.; Starikov, A. G.; Starikova, A. A. Computational Insight into Magnetic Behavior and Properties of the Transition Metal Complexes with Redox-Active Ligands: A DFT Approach. *Pure Appl. Chem.* **2018**, *90*, 811–824.

(54) Starikova, A. A.; Minkin, V. I. Adducts of Transition Metal Complexes with Redox-Active Ligands: The Structure and Spin-State-Switching Rearrangements. *Russ. Chem. Rev.* **2018**, *87*, 1049–1079.

(55) Wang, J. P.; Liu, W. T.; Yu, M.; Ji, X. Y.; Liu, J. L.; Chi, M. Z.; Starikova, A. A.; Tao, J. One-Step versus Two-Step Valence Tautomeric Transitions in Tetraoxolene-Bridged Dinuclear Cobalt Compounds. *Inorg. Chem.* **2022**, *61*, 4428–4441.

(56) Hammett, L. P. The Effect of Structure upon the Reactions of Organic Compounds. Temperature and Solvent Influences. *J. Chem. Phys.* **1936**, *4*, 613–617.

(57) Genix, P.; Jullien, H.; Le Goas, R. Estimation of Hammett Sigma Constants from Calculated

Atomic Charges Using Partial Least Squares Regression. *J. Chemom.* **1996**, *10*, 631–636.

(58) Noodleman, L. Valence Bond Description of Antiferromagnetic Coupling in Transition Metal Dimers. *J. Chem. Phys.* **1981**, *74*, 5737–5743.

(59) Gransbury, G. K.; Boulon, M.-E.; Mole, R. A.; Gable, R. W.; Moubaraki, B.; Murray, K. S.; Sorace, L.; Soncini, A.; Boskovic, C. Single-Ion Anisotropy and Exchange Coupling in Cobalt(II)-Radical Complexes: Insights from Magnetic and Ab Initio Studies. *Chem. Sci.* **2019**, *10*, 8855–8871.

(60) Starikov, A. G.; Starikova, A. A.; Minkin, V. I. Quantum-Chemical Study of Spin Crossover in Cobalt Complexes with an o-Benzoquinone Ligand. *Dokl. Chem.* **2016**, *467*, 83–87.

(61) Khusniyarov, M. M.; Harms, K.; Burghaus, O.; Sundermeyer, J. Molecular and Electronic Structures of Homoleptic Nickel and Cobalt Complexes with Non-Innocent Bulky Diimine Ligands Derived from Fluorinated 1,4-Diaza-1,3-butadiene (DAD) and Bis(Arylimino)Acenaphthene (BIAN). *Eur. J. Inorg. Chem.* **2006**, *2006*, 2985–2996.

(62) Cowieson, N. P.; Aragao, D.; Clift, M.; Ericsson, D. J.; Gee, C.; Harrop, S. J.; Mudie, N.; Panjikar, S.; Price, J. R.; Riboldi-Tunnicliffe, A.; Williamson, R.; Caradoc-Davies, T. MX1: A Bending-Magnet Crystallography Beamline Serving Both Chemical and Macromolecular Crystallography Communities at the Australian Synchrotron. *J. Synchrotron Radiat.* **2015**, *22*, 187–190.

(63) Aragão, D.; Aishima, J.; Cherukuvada, H.; Clarken, R.; Clift, M.; Cowieson, N. P.; Ericsson, D. J.; Gee, C. L.; Macedo, S.; Mudie, N.; Panjikar, S.; Price, J. R.; Riboldi-Tunnicliffe, A.; Rostan, R.; Williamson, R.; Caradoc-Davies, T. T. MX2: A High-Flux

Undulator Microfocus Beamline Serving Both the Chemical and Macromolecular Crystallography Communities at the Australian Synchrotron. *J. Synchrotron Radiat.* **2018**, *25*, 885–891.

(64) Camargo, P. H. C. The Chemical Bond in Inorganic Chemistry: The Bond Valence Model, 2nd Ed. *J. Mater. Sci.* **2017**, *52*, 9959–9962.

(65) Ketkaew, R.; Tantirungrotechai, Y.; Harding, P.; Chastanet, G.; Guionneau, P.; Marchivie, M.; Harding, D. J. OctaDist: A Tool for Calculating Distortion Parameters in Spin Crossover and Coordination Complexes. *Dalton Trans.* **2021**, *50*, 1086–1096.

(66) Llunell, M.; Casanova, D.; Cirera, J.; Alemany, P.; Alvarez, S. SHAPE, 2.1. Universitat de Barcelona: Barecelona, Spain 2013.

(67) Fedushkin, I. L.; Lukoyanov, A. N.; Baranov, E. V. Lanthanum Complexes with a Diimine Ligand in Three Different Redox States. *Inorg. Chem.* **2018**, *57*, 4301–4309.

(68) Zhou, M.; Li, X.; Bu, D.; Lei, H. Synthesis, Crystal Structures and Electrochemical Properties of Co(II) and Mn(II) Complexes with Asymmetric Bulky BIAN Ligands. *Polyhedron* **2018**, *148*, 88–99.

(69) Zarkesh, R. A.; Ichimura, A. S.; Monson, T. C.; Tomson, N. C.; Anstey, M. R. Voltage Clustering in Redox-Active Ligand Complexes: Mitigating Electronic Communication through Choice of Metal Ion. *Dalton Trans.* **2016**, *45*, 9962–9969.

(70) Brown, I. D.; Altermatt, D. Bond-Valence Parameters Obtained from a Systematic Analysis of the Inorganic Crystal Structure Database. *Acta Crystallogr. Sect. B Struct. Sci.* **1985**, *244*, 244–247.

(71) Halcrow, M. A. Jahn–Teller Distortions in Transition Metal Compounds, and Their Importance in Functional Molecular and Inorganic Materials. *Chem. Soc. Rev.* **2013**, *42*, 1784–1795.

(72) Coventry, D. N.; Batsanov, A. S.; Goeta, A. E.; Howard, J. A. K.; Marder, T. B. Synthesis and Molecular Structures of α-Diimines and Their Zinc and Palladium Dichloride Complexes. *Polyhedron* **2004**, *23*, 2789–2795.

(73) Mondal, P.; Agarwala, H.; Jana, R. D.; Plebst, S.; Grupp, A.; Ehret, F.; Mobin, S. M.; Kaim, W.; Lahiri, G. K. Sensitivity of a Strained C–C Single Bond to Charge Transfer: Redox Activity in Mononuclear and Dinuclear Ruthenium Complexes of Bis(Arylimino)Acenaphthene (BIAN) Ligands. *Inorg. Chem.* **2014**, *53*, 7389–7403.

(74) Caneschi, A.; Dei, A.; Gatteschi, D.; Tangoulis, V. Antiferromagnetic Coupling in a Six-Coordinate High Spin Cobalt(II)-Semiquinonato Complex. *Inorg. Chem.* **2002**, *41*, 3508–3512.

(75) Liang, H. W.; Kroll, T.; Nordlund, D.; Weng, T. C.; Sokaras, D.; Pierpont, C. G.; Gaffney, K. J. Charge and Spin-State Characterization of Cobalt Bis(o-Dioxolene) Valence Tautomers Using Co Kβ x-Ray Emission and l-Edge x-Ray Absorption Spectroscopies. *Inorg. Chem.* **2017**, *56*, 737–747.

(76) Protasenko, N. A.; Poddel'Sky, A. I.; Bogomyakov, A. S.; Somov, N. V.; Abakumov, G. A.; Cherkasov, V. K. Bis-o-Semiquinonato Complexes of Transition Metals with 5,7-Di-Tert-Butyl-2-(Pyridine-2-Yl)Benzoxazole. *Polyhedron* **2013**, *49*, 239–243.

(77) Bowman, A. C.; Milsmann, C.; Bill, E.; Lobkovsky, E.; Weyhermüller, T.; Wieghardt, K.;

Chirik, P. J. Reduced N -Alkyl Substituted Bis(Imino)Pyridine Cobalt Complexes: Molecular and Electronic Structures for Compounds Varying by Three Oxidation States. *Inorg. Chem.* **2010**, *49*, 6110–6123.

(78) Hiller, M.; Sittel, T.; Wadepohl, H.; Enders, M. A New Class of Lanthanide Complexes with Three Ligand Centered Radicals: NMR Evaluation of Ligand Field Energy Splitting and Magnetic Coupling. *Chem. – A Eur. J.* **2019**, *25*, 10668–10677.

(79) Tsukerblat, B. S.; Tarantul, A.; Müller, A. Antisymmetric Exchange and Pseudo Jahn-Teller Instability in Spin-Frustrated Metal Clusters. *J. Mol. Struct.* **2007**, *838*, 124–132.

(80) Van Den Heuvel, W.; Chibotaru, L. F. Elucidation of the Magnetism of $[Co_2PdCl_2(Dpa)_4]$: Origin of a Large Temperature Domain of TIP Behavior. *Inorg. Chem.* **2009**, *48*, 7557–7563.

(81) Rohmer, M. M.; Liu, I. P. C.; Lin, J. C.; Chiu, M. J.; Lee, C. H.; Lee, G. H.; Bénard, M.; López, X.; Peng, S. M. Structural, Magnetic, and Theoretical Characterization of a Heterometallic Polypyridylamide Complex. *Angew. Chem., Int. Ed.* **2007**, *46*, 3533–3536.

(82) Fedushkin, I. L.; Maslova, O. V.; Baranov, E. V.; Shavyrin, A. S. Redox Isomerism in the Lanthanide Complex $[(Dpp\text{-}Bian)Yb(DME)(\mu\text{-}Br)]_2$ (Dpp-Bian = 1,2-Bis[(2,6-Diisopropylphenyl)Imino]Acenaphthene). *Inorg. Chem.* **2009**, *48*, 2355–2357.

(83) Nadurata, V. L.; Boskovic, C. Switching Metal Complexes via Intramolecular Electron Transfer: Connections with Solvatochromism. *Inorg. Chem. Front.* **2021**, *8*, 1840–1864.

(84) Fedushkin, I. L.; Skatova, A. A.; Chudakova, V. A.; Cherkasov, V. K.; Fukin, G. K.; Lopatin, M. A. Reduction of 1,2-Bis[(2,6-Diisopropylphenyl)Imino]Acenaphthene (Dpp-

Bian) with Alkali Metals− A Study of the Solution Behaviour of (Dpp-Bian)N−[M+]n (M = Li, Na;n = 1−4) with UV/Vis, ESR And1H NMR Spectroscopy. *Eur. J. Inorg. Chem.* **2004**, *2004*, 388–393.

(85) Robin, Melvin B.; Day, P. Mixed Valence Chemistry-A Survey and Classification. *Adv. Inorg. Chem. Radiochem.* **1967**, *10*, 247–422.

(86) Creutz, C. Mixed Valence Complexes of d 5 - d 6 Metal Centers. In *Progress in Inorganic Chemistry*; 2007; pp 1–73.

(87) Arnold, A.; Sherbow, T. J.; Sayler, R. I.; Britt, R. D.; Thompson, E. J.; Muñoz, M. T.; Fettinger, J. C.; Berben, L. A. Organic Electron Delocalization Modulated by Ligand Charge States in [L2M]n- Complexes of Group 13 Ions. *J. Am. Chem. Soc.* **2019**, *141*, 15792–15803.

(88) Mörtel, M.; Oschwald, J.; Scheurer, A.; Drewello, T.; Khusniyarov, M. M. Molecular Valence Tautomeric Metal Complexes for Chemosensing. *Inorg. Chem.* **2021**, *60*, 14230–14237.

(89) Hearns, N. G. R.; Korčok, J. L.; Paquette, M. M.; Preuss, K. E. Dinuclear Cobalt Bis(Dioxolene) Complex Exhibiting Two Sequential Thermally Induced Valence Tautomeric Transitions. *Inorg. Chem.* **2006**, *45*, 8817–8819.

(90) Witt, A.; Heinemann, F. W.; Sproules, S.; Khusniyarov, M. M. Modulation of Magnetic Properties at Room Temperature: Coordination-Induced Valence Tautomerism in a Cobalt Dioxolene Complex. *Chem. - Eur. J.* **2014**, *20*, 11149–11162.

SYNPOSIS

Guided by density functional theory calculations, variation of the redox-state and aryl substituents in a series of homoleptic $[Co(Ar\text{-}BIAN)_3]^{n+}$ (bis((aryl)imino)acenapthene) complexes has afforded a thermally-induced valence tautomeric interconversion in acetonitrile solution for neutral $[Co(4\text{-}MeO\text{-}Ph\text{-}BIAN)_3]$ (4MeO-Ph-BIAN = bis[N,N'-(4-methoxy-phenyl)imino]acenaphthene).